NACA

RESEARCH MEMORANDUM

PRELIMINARY INVESTIGATION OF THE TRANSONIC CHARACTERISTICS OF AN NACA SUBMERGED INLET

By John A. Axelson and Robert A. Taylor

Ames Aeronautical Laboratory
Moffett Field, Calif.

NATIONAL ADVISORY COMMITTEE
FOR AERONAUTICS

WASHINGTON
June 5, 1950

NATIONAL ADVISORY COMMITTEE FOR AERONAUTICS

RESEARCH MEMORANDUM

PRELIMINARY INVESTIGATION OF THE TRANSONIC CHARACTERISTICS OF AN NACA SUBMERGED INLET

By John A. Axelson and Robert A. Taylor

SUMMARY

A preliminary investigation of an NACA submerged inlet operating over a range of mass-flow ratios and oncoming flow angles was conducted through a Mach number range from 0.70 to 1.15 by the use of a transonic bump. Ram recovery and pressure distribution were measured for mass-flow ratios up to 0.67. For approximately constant mass-flow ratio, the ram-recovery ratio decreased about 0.05 in the Mach number range from 0.85 to 1.1, but generally improved above a Mach number of 1.0 or 1.1. The ram-recovery ratio decreased about 0.05 when the angle between the inlet center plane and the free stream was increased from 0° to 4°, but increased about 0.02 from this reduced value when the angle was increased from 4° to 8°. Increasing the mass flow into the inlet increased the ram recovery, but the improvement became progressively less at the higher mass flows and higher Mach numbers. Static-pressure and total-pressure surveys inside the inlet indicated that the losses in ram recovery were caused principally by the entrance of low-energy air from the surrounding boundary layer which passed over the sharp edges of the ramp walls and mixed with the higher-energy air entering the inlet.

INTRODUCTION

The location of air inlets on the sides of the fuselages of jet-propelled aircraft has received special emphasis recently because of the necessity of housing radar and armament in the fuselage noses. Although a side location generally introduces boundary-layer problems, a distinct advantage is gained by the shorter internal ducting from the air inlet to the compressor. As a result of wind-tunnel tests directed toward the development of a side inlet having high pressure-recovery characteristics and minimum adverse effects from the fuselage boundary layer, the NACA submerged inlet was conceived. Several variations of this inlet were investigated in one of the Ames 7- by 10-foot wind tunnels and are discussed in reference 1. A design judged from the results of those tests to be optimum was then tested on a wing-body combination in the Ames

16-foot high-speed wind tunnel up to a free-stream Mach number of 0.875. This free-stream Mach number corresponded to slightly higher local Mach numbers at the inlet, depending upon the location of the inlet with respect to the wing and fuselage. (See reference 2.) The preliminary investigation reported herein was conducted using an identical inlet mounted on an almost flat, two-dimensional surface of a transonic bump in the Ames 16-foot high-speed wind tunnel. For these tests the local Mach number over the bump in the region of the inlet ranged from 0.70 to 1.15.

NOTATION

The symbols used in this report and their definitions are as follows:

A	cross-sectional area of duct, square inches
d	inlet depth, 1.6 inches
H	total pressure, pounds per square foot
h	boundary-layer parameter designating the height for which a complete loss of dynamic pressure $\left(\frac{1}{2}\rho U_o^2\right)$ would be equivalent to the integrated loss of total pressure in the actual boundary layer $\left[\frac{1}{H_o - p_o}\int_o^\infty (H_o - H)dy\right]$, inches
M	Mach number
m	mass flow (ρAu), slugs per second
P	pressure coefficient $\left(\frac{p - p_o}{q_o}\right)$
p	static pressure, pounds per square foot
q	dynamic pressure $\left(\frac{1}{2}\rho U^2\right)$, pounds per square foot
U	velocity outside boundary layer, feet per second
u	local velocity, feet per second
y	increment of boundary-layer thickness, inches
$\frac{A_e}{A_1}$	ratio of duct cross-sectional area 12 inches downstream of lip leading edge to cross-sectional area at rake

$\frac{H_1 - p_o}{H_o - p_o}$ ram-recovery ratio

$\frac{m_1}{m_o}$ ratio of the mass flow through the inlet to the mass flow in the free stream through an area equal to the inlet area $\left(\frac{\rho_1 A_1 u_1}{\rho_o A_1 U_o}\right)$

α angle between the inlet center plane and the free stream (simulating the angle of attack of an airplane side inlet), degrees

δ boundary-layer thickness where the local velocity is 0.99 of the velocity outside the boundary layer, inches

δ^* boundary-layer displacement thickness $\left[\int_o^\infty \left(1 - \frac{\rho u}{\rho_o U_o}\right) dy\right]$, inches

θ boundary-layer momentum thickness $\left[\int_o^\infty \frac{\rho u}{\rho_o U_o}\left(1 - \frac{u}{U_o}\right) dy\right]$, inches

ρ mass density, slugs per cubic foot

Subscripts

o average conditions over test section of bump

e diffuser entrance

1 duct rake

APPARATUS

Description of Inlet Models

Details and dimensions of the NACA submerged-inlet model are shown in figure 1. Insofar as possible, the dimensions of the inlet corresponded to those of the inlet reported in reference 2, where the inlet was installed on the curved side of a model fuselage. In the present investigation, the inlet was mounted on a two-dimensional surface as shown in figure 2. To simulate angle-of-attack conditions of an airplane

side inlet, the inlet was mounted on the transonic bump with angles of 0°, 4°, and 8° between the inlet center plane and the free stream. The curvature of the test surface necessitated the construction and installation of three separate models with identical basic inlet lines.

The models were equipped with pressure orifices along the center line of the ramp and around the lip (except the inlet representing 8° angle of attack which had no lip orifices). Pressure losses and flow rates in the inlet were measured with a rake 6 inches behind the lip leading edge. The rake consisted of 30 total-pressure and 35 static-pressure tubes. The air which flowed through the inlet entered a diffuser which started 6 inches downstream of the rake and discharged back to the wind-tunnel air stream through the underside of the bump.

Description of the Transonic Bump

The transonic bump of the Ames 16-foot high-speed wind tunnel used for testing models through sonic velocity and up to low supersonic speeds is shown in figure 3. The bump had an 18-foot chord and a flat underside which was mounted a small distance away from one of the vertical walls of the wind tunnel. The profile of the bump was essentially one-half of an NACA 16-021 section modified by a 17-percent extension of the chord and faired by a straight line connecting the 64-percent-chord point of the resulting profile to the trailing edge.

Distributions of local Mach number over the bump surface are shown in figure 4. At the highest Mach numbers, there was an increase in the local Mach number and consequently a small favorable pressure gradient along that portion of the bump surface in which the submerged inlet was placed. The magnitude of the favorable pressure gradient on the bump was, however, small compared to the gradient of pressure along the ramp of the inlet, amounting to less than 3 percent of the gradient on the ramp below a Mach number of 1.05, and less than 7 percent at the highest Mach numbers. Thus, the gradient of Mach number was felt to have only a small effect on the results obtained for the inlet, and was of a magnitude which could conceivably exist along the side of the fuselage of an airplane.

The underside of the bump was mounted a small distance away from the vertical wall of the wind tunnel in order that the boundary layer of the tunnel wall would pass under the bump. A 2-inch spacing existed during the tests of the inlet at 0° angle of attack. When the inlet was tested at 4° and 8° angles of attack, the spacing was increased to 5 inches in order to reduce the boundary layer on the bump and to decrease the static pressure under the bump so that slightly higher mass flows through the inlet might be obtained. (The duct exhausted through the underside of the bump.) Results of boundary-layer surveys 7 inches

forward of the ramp at bump station 73.3 are presented in figure 5 for the bump located 2 inches and 5 inches from the wind-tunnel wall. The bump boundary layer was decreased by increasing the spacing, but time did not permit repeating the tests of the inlet at 0° angle of attack with the 5-inch spacing.

TESTS

A Mach number range from 0.70 to 1.15 was covered in the investigation of the inlets, the Mach numbers being taken as the average of the values prevailing between bump stations 78 and 114 inches. Under the test conditions, this range of Mach numbers corresponded to a Reynolds number range from 3.5 to 4.2 million per foot of length.

Three different mass-flow conditions were investigated with the inlet at 0° angle of attack. The two reduced flow rates were produced by the addition of constrictions 13 inches behind the lip in the diffuser entrance. Since rigid control of the mass flow during the tests was not practicable, there were small variations in the resulting mass-flow ratios over the Mach number range. Only one mass-flow condition was investigated at 4° and 8° angles of attack.

RESULTS AND DISCUSSION

Ram-Recovery Ratio

The ram-recovery ratios were computed by the method outlined in reference 2 wherein the logarithms of the local total pressures at each of the 30 total-pressure tubes of the rake were weighted according to the local mass flows.

The primary variables which affect the ram recovery of the inlet and which can be isolated in the present investigation are mass-flow ratio, angle of attack, boundary-layer profile, and Mach number. The effects of each of these on the ram recovery will be discussed.

Effect of mass-flow ratio.- The variations of ram-recovery and mass-flow ratios with Mach number for three different diffuser-entrance constrictions are shown in figure 6 for the inlet at an angle of attack of 0°. A cross plot of these results is presented in figure 7. At all test Mach numbers increasing the mass-flow ratio resulted in an increased ram recovery, but the improvement generally became progressively smaller at the higher mass-flow ratios and at the higher Mach numbers. These results are in agreement with those measured during the investigation reported in

reference 2 wherein the optimum mass-flow ratio was about 0.70 over the Mach number range from 0.30 to 0.875. Since only one flow condition was tested with the inlet at angles of attack of 4° and 8°, it was not possible to present the ram-recovery ratios for these angles of attack at constant values of mass-flow ratio. The amount by which the mass-flow ratios varied, however, were not large enough to obscure the consistent trend in the variation of ram-recovery ratio with Mach number.

Effect of angle of attack.- The variations with Mach number of ram-recovery ratio and mass-flow ratio for angles of attack of 0°, 4°, and 8° are shown in figure 8. Because of the difference in spacing between the underside of the bump and the wind-tunnel wall, slightly higher mass flows were obtained with the inlet at 4° and 8° angles of attack than were obtained with the inlet at 0° angle of attack. The mass-flow ratios shown in figure 8(b) are not to be compared for evaluation of an effect of angle of attack, but are shown in order that a comparison can be made between the ram-recovery ratios shown in figure 8(a). Had the same bump spacing been used for all three angles of attack the mass flows would in all probability have been nearly equal at any given Mach number. The small differences in measured mass flows between the 4° and 8° angles of attack were probably within the accuracy of the test results.

The results show, at least qualitatively, that the ram-recovery ratios for the 4° and 8° angles of attack were slightly less than those for 0° angle of attack in spite of the fact that the mass-flow ratios were higher by 0.02 to 0.09. A comparison probably more quantitative in nature is possible by performing an extrapolation of the results shown in figure 6 for the inlet at 0° angle of attack so that the ram-recovery ratios for three angles of attack might be compared on the basis of equal mass-flow ratio. (The results presented in figure 8 of reference 2 which cover higher mass-flow ratios than those covered in the present investigation indicate that serious error is unlikely in making such an extrapolation.) For example, in the present investigation at a Mach number of 0.95 the ram-recovery ratio for 0° angle of attack extrapolated up to a mass-flow ratio of 0.62, the value shown in figure 8(b) for 4° and 8° angles of attack corresponds to a value of about 0.83; but introducing this value in figure 8(a) has little effect on the relative values of the ram-recovery ratios for the three angles of attack. At comparable mass-flow ratios, the ram-recovery ratio decreased about 0.05 when the angle of attack was increased from 0° to 4°, but improved about 0.02 when the angle of attack was increased from 4° to 8°. A similar variation of ram-recovery ratio with angle of attack was reported in figure 9 of reference 2 for the inlet fitted with small boundary-layer deflectors shown in figure 3 of reference 2.

Effect of Mach number and bump boundary layer.- The determination of the ram-recovery characteristics of an NACA submerged inlet through the transonic speed range was the primary purpose of the present investigation and the results have been presented in figures 6(a), 7, and 8(a). The

effects upon ram-recovery ratio of variations of the mass-flow ratio and of the angle of attack have been discussed, leaving the effects of Mach number to be isolated. Since the results presented in figure 5 indicate that changes occurred in the boundary layer on the bump when the Mach number was varied, it is desirable to ascertain what effect the boundary-layer changes exerted on the ram-recovery characteristics of the inlet.

As shown in figure 5(d), the maximum change in the boundary-layer parameter h/d throughout the test range of Mach numbers was about 0.025, most of which occurred below 0.92 Mach number. The results from the present investigation have been combined in figure 9 with those from reference 2 and show the relationship between the boundary-layer parameter h/d and the ram-recovery ratio of the inlet. The results for the three Mach numbers for which the two investigations overlapped indicate that the 0.025 change in h/d could cause an increment of ram-recovery ratio of about 0.02. However, in the present investigation, the boundary-layer parameter h/d remained almost constant above 0.92 Mach number, while the most significant changes in ram-recovery ratio occurred above this Mach number. It appears, then, that in analyzing the variation of ram-recovery ratio with Mach number for Mach numbers above 0.92 it is permissible to consider the bump boundary layer essentially constant, thereby allowing further scrutiny of the effects of Mach number.

The results in figure 9, in addition to providing evidence on the effect of the changes in the boundary layer, also serve to correlate the ram-recovery results of reference 2 with those of the present investigation. Perhaps more important, however, the results in figure 9 show how large an effect the energy deficiency in the oncoming boundary layer exerted on the ram-recovery characteristics of the inlet.

It has been shown that the effects of changes in the mass-flow ratio and in the bump boundary layer above 0.92 Mach number were too small to mask the consistent reductions in ram-recovery ratio which occurred at Mach numbers near 1.0 and the slight improvement above 1.1 Mach number. Information on the changes in the flow into the inlet which accompanied the changes in the Mach number is introduced in the following sections, which present the distributions of the losses in the inlet, photographs of tufts on the model, and pressure distributions.

Distribution of ram-recovery losses inside the inlet.- In order to show the distribution of the ram-recovery losses within the inlet, contours of the computed local ram-recovery and mass-flow ratios are presented in figures 10, 11, and 12. The results are arranged to show primarily the effects of Mach number, the mass-flow ratios for each set of three Mach numbers being chosen as nearly equal as possible from the available data.

The results shown in figure 10, the integrated values of which appeared in figure 6, cover three mass-flow conditions for 0° angle of

attack. As would be expected, the regions of high ram recovery corresponded to those of high mass flow. In general, the losses were concentrated in those areas adjacent to the ramp and in the corners where boundary layers were to be expected. The asymmetry of flow and of losses which were more evident at the lowest mass flow (fig. 10(g)) was probably caused by small differences between the boundary layers in the upper and lower portions of the inlet rather than by a change in the flow direction over the inlet, inasmuch as the latter would have had a similar effect on the results at the higher mass flows and, further, tuft studies indicated no change in flow direction over the bump.

The ram-recovery and mass-flow contours for angles of attack of 4° and 8° are shown in figures 11 and 12. As might be expected, there was a concentration of the losses in the lower portion of the inlet because of the differences in the direction and spillage of air and in the boundary layers along the two diverging ramp walls. Differences in the boundary layers would be expected in light of the differences in the pressure distributions presented in figure 13, which were measured during the investigation reported in reference 2. These results show large differences between the local pressures along the two walls when the inlet was operating at other than zero angle of attack.

Cause of the losses.- In reference 3, it was surmised from ram-recovery distributions for a similar inlet that the flow of air over the sharp edges of the ramp walls and into the inlet imparted a rotational velocity component to the air. It was reasoned that this rotational velocity increased with mass-flow ratio and with the divergence of the ramp walls relative to the direction of the air stream and resulted in the formation of one or more vortices, the centers of which produced regions of low local ram recovery not immediately adjacent to the walls. In the present investigation, similar regions of ram-recovery losses were measured, such as those shown in figures 11(a) and 12(a). In order to provide more information on the nature of the ram-recovery losses, the contours of figure 11(a) are compared with the measured total and static pressures across the inlet in figure 14. In light of the results shown in figure 9 and the large variations in total pressure across the inlet, it appears logical to attribute the regions of ram-recovery loss and low total pressure to the deficiency of energy in the air which came from the bump boundary layer and left the surface in passing over the sharp edges of the ramp wall before reaching the inlet. Only relatively small variations of static pressure across the inlet and no marked reductions in local static pressure such as might be expected at the core of a vortex were measured in the present investigation, so it is possible that the rotational velocity components remained as more or less random vorticity or turbulence. It is also possible that, at the mass-flow ratios covered in the present investigation, the cores of the vortices passed outside the inlet. The latter would explain condensation trails which were observed in the wind tunnel during the course of the tests. With higher mass-flow ratios than were obtained in the present investigation, it is

possible that the rotational velocity components could wrap up into vortices which would enter the inlet. On the basis of the present investigation, however, it is felt that the losses in ram recovery were, in the most part, caused by the entry of air from the bump boundary layer.

The divergent ramp of the NACA submerged inlet appears to offer two advantages with respect to the boundary layer in which it is placed. First, the oncoming boundary layer that flows directly on to the ramp does not thicken, as it approaches the inlet, in correspondence with the adverse pressure gradient it encounters because the diverging walls provide relief in a third dimension; and, second, the boundary layer that flows from the outside surface on to the ramp by passing over the sharp edges of the ramp wall is involved in a mixing action with higher-energy air and so is less prone to separate.

Pressure Distributions and Tuft Studies

In the preceding discussion, the ram-recovery losses were attributed principally to the entrance of low-energy air from the bump boundary layer. The bump boundary-layer parameters varied comparatively little above 0.92 Mach number; however, the ram-recovery ratios varied in the Mach number range from 0.92 to 1.15. Tuft studies, some photographs of which are presented in figure 15, indicated that no significant separation occurred on the ramp. It appears logical, then, to attribute the variations in ram-recovery ratio with Mach number primarily to changes in the amounts of low-energy air which entered the inlet from the surrounding bump boundary layer. The controlling factor which determined the amount of bump boundary-layer air which entered the inlet was the local pressure gradient between the ramp and the surrounding bump surface. Pressure distributions along the ramp, some of which appear in figures 16 and 17, indicate that the pressure differences were generally greatest and extended over longer portions of the ramp at the Mach numbers corresponding to those at which the minimum ram-recovery ratios were measured. (See figs. 7 and 8.)

The effect of variation in mass-flow ratio on the pressure distributions along the center line of the ramp and around the lip is also shown in figure 16 for an angle of attack of 0° at Mach numbers of approximately 0.75, 1.02, and 1.14. Reduction of mass flow at the higher Mach numbers had the expected effects of increasing the pressures on the ramp and increasing the angle of attack at which the lip operated. Figure 17 presents additional pressure distributions along the ramp for angles of attack of 0°, 4°, and 8° and around the lip for 0° and 4°. Varying the angle of attack with a constant mass flow had a noticeable effect on the pressures around the lip, but had little effect on the pressures along the center line of the ramp. It should be repeated, however, that variation of angle of attack produced large changes in the pressures along the ramp walls as shown in figure 13.

Since the pressure distributions and tuft studies indicated that the entrance of air from the oncoming boundary layer occurred principally over the forward part of the ramp walls where the local pressures were less than those of the surrounding air stream, it appears that, if boundary-layer control were to be employed, the surrounding surface just outside and forward of the ramp should be considered in addition to the surface of the ramp itself. The tufts shown in figures 15(a) and 15(b) indicate that the boundary layer along the after part of the ramp walls passed outside of the lip in the direction of the local pressure gradient.

CONCLUSIONS

The following conclusions were drawn from the results of tests of an NACA submerged inlet on a transonic bump for a test Mach number range from 0.70 to 1.15:

1. For mass-flow ratios between 0.40 and 0.67, the ram-recovery ratio decreased about 0.05 in the Mach number range from 0.85 to roughly 1.1. Generally there was a small improvement in the ram-recovery ratio at Mach numbers above 1.0 or 1.1.

2. For comparable mass-flow ratios, the ram-recovery ratio decreased about 0.05 when the angle of attack was increased from 0° to 4°, but improved about 0.02 when the angle of attack was increased from 4° to 8°.

3. Increasing the mass-flow ratio resulted in higher ram-recovery ratios but, in general, the improvement became progressively less at the higher mass flows and Mach numbers investigated.

4. Ram-recovery ratios higher than those obtained in the present investigation appear possible on installations with relatively thinner boundary layers.

Ames Aeronautical Laboratory,
National Advisory Committee for Aeronautics,
Moffett Field, Calif.

[redacted]

REFERENCES

1. Mossman, Emmet A., and Randall, Lauros M.: An Experimental Investigation of the Design Variables for NACA Submerged Duct Entrances. NACA RM A7I30, 1948.

2. Hall, Charles F., and Barclay, F. Dorn: An Experimental Investigation of NACA Submerged Inlets at High Subsonic Speeds. I – Inlets Forward of the Wing Leading Edge. NACA RM A8B16, 1948.

3. Delany, Noel K.: An Investigation of Submerged Air Inlets on a 1/4-Scale Model of a Typical Fighter-Type Airplane. NACA RM A8A20, 1948.

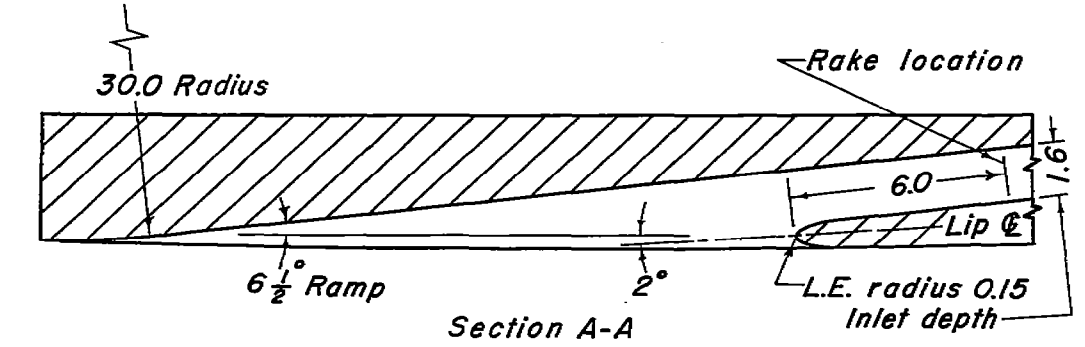

Section A-A

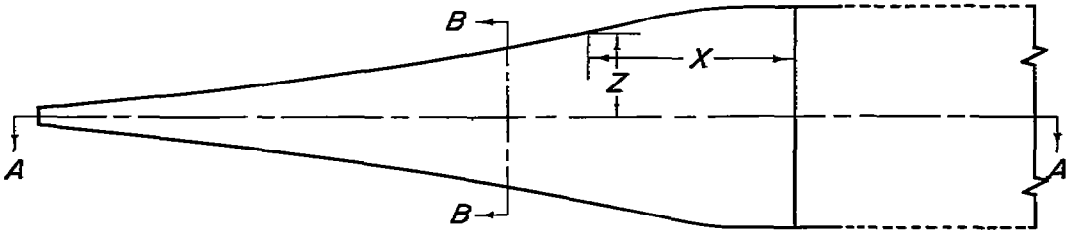

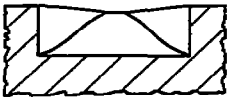

Section B-B

Lip Coordinates

Station	Outer surface	Inner surface
Inches from nose	Inches from lip center line	Inches from lip center line
0	0	0
.20	.195	.195
.40	.270	.270
.60	.322	.331
.80	.357	.377
1.00	.384	.409
1.20	.405	.432
1.40	.423	.444
1.60	.438	.450
1.80	.453	.453

Note: All dimensions in inches

Ramp-Wall Coordinates

X, Inches	Z, Inches
0	3.20
2.11	3.18
4.22	2.93
6.33	2.45
8.44	1.94
10.55	1.55
12.66	1.25
14.77	.99
16.88	.75
18.99	.51
21.15	.27

Figure 1.- Dimensional data for model inlet.

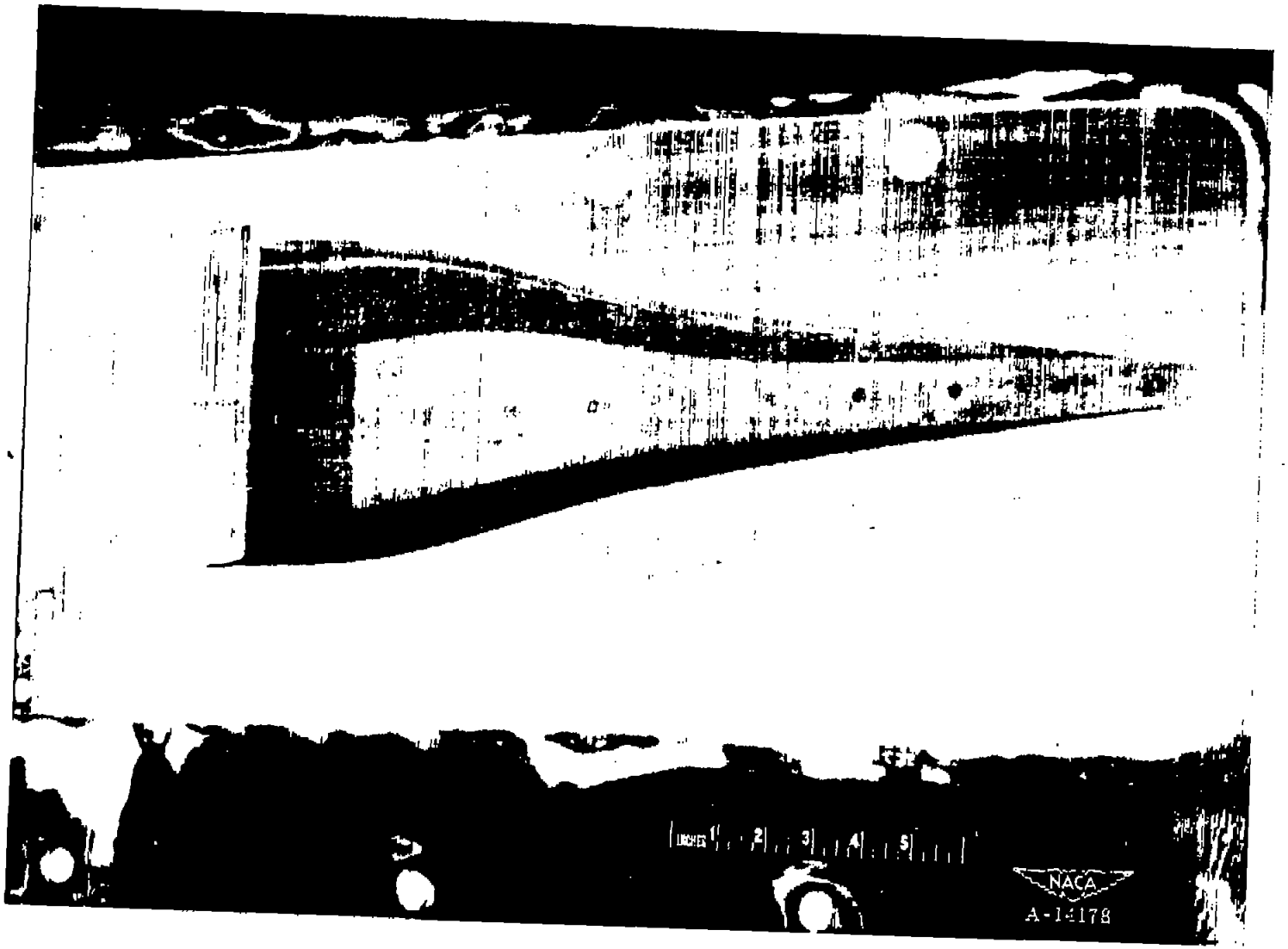

Figure 2.- Model of NACA submerged inlet.

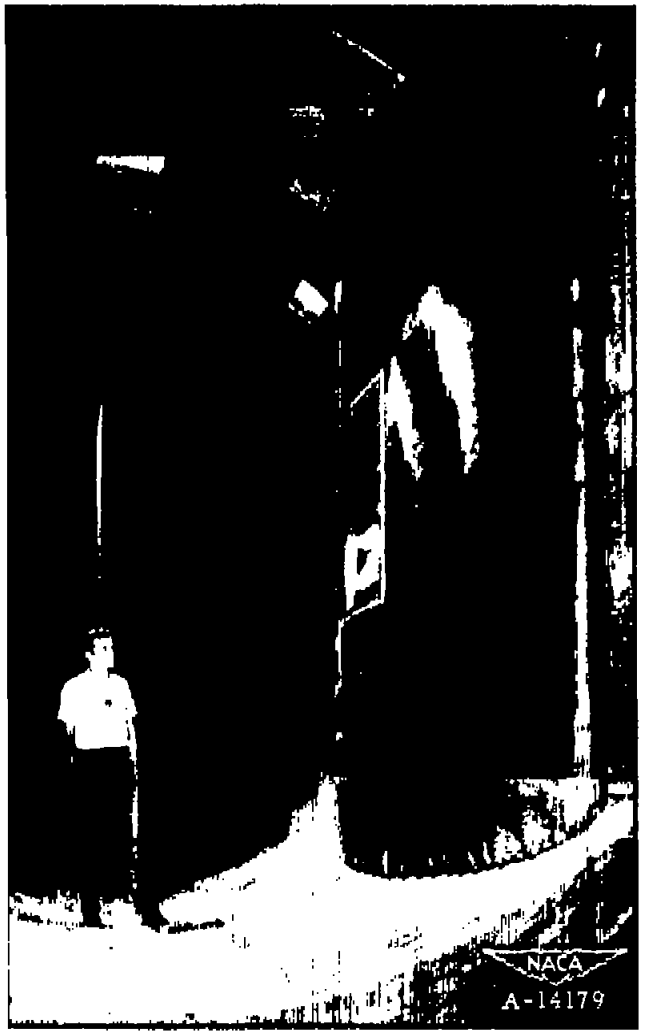

(a) Upstream view.

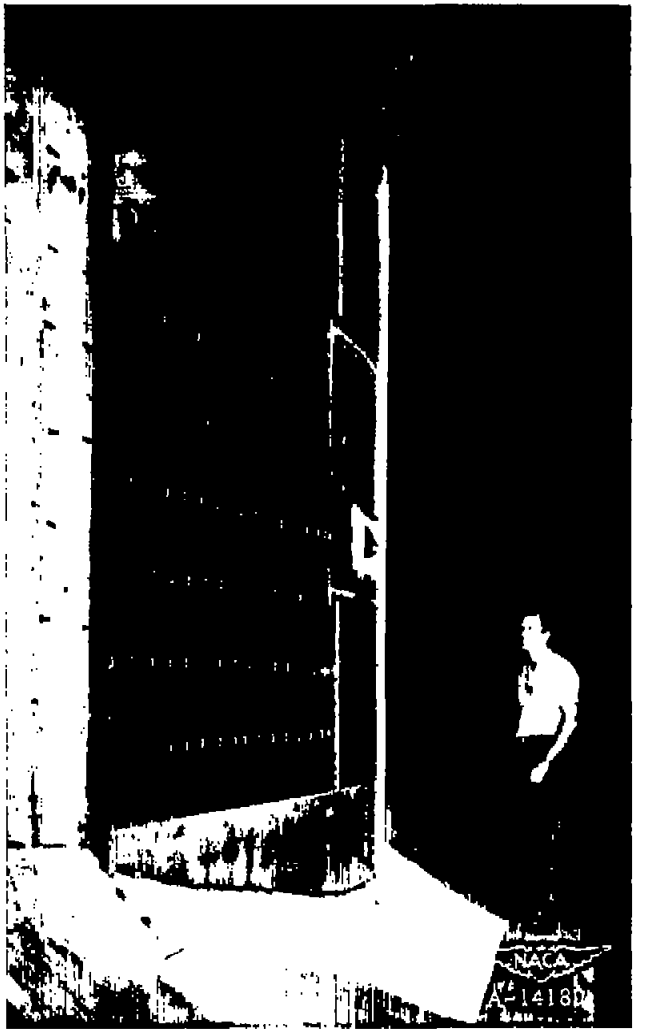

(b) Downstream view.

Figure 3.- Model of NACA submerged inlet mounted on the transonic bump in the Ames 16-foot high-speed wind tunnel.

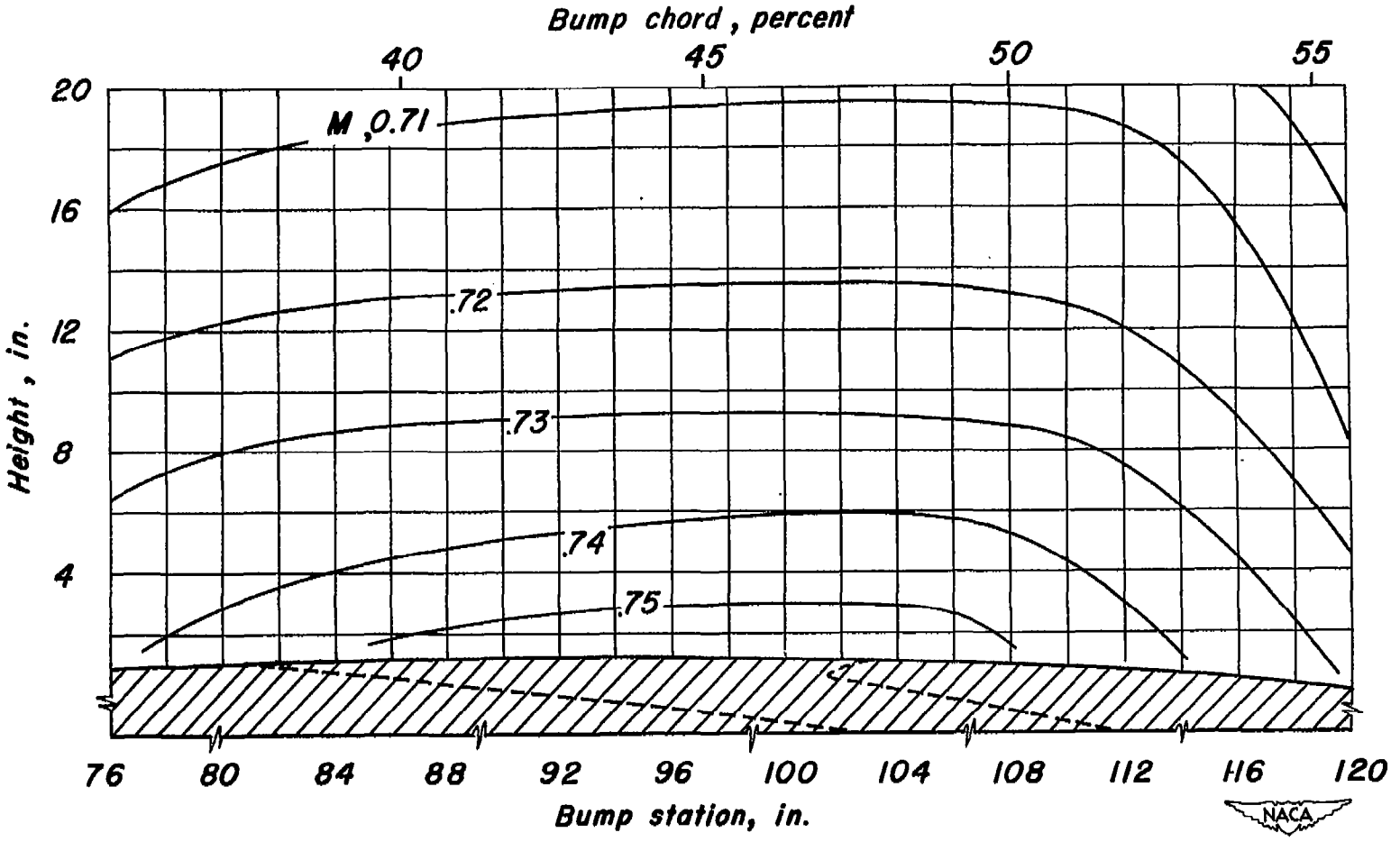

(a) M_∞, 0.75

Figure 4.– Mach number distribution perpendicular to the surface of the transonic bump.

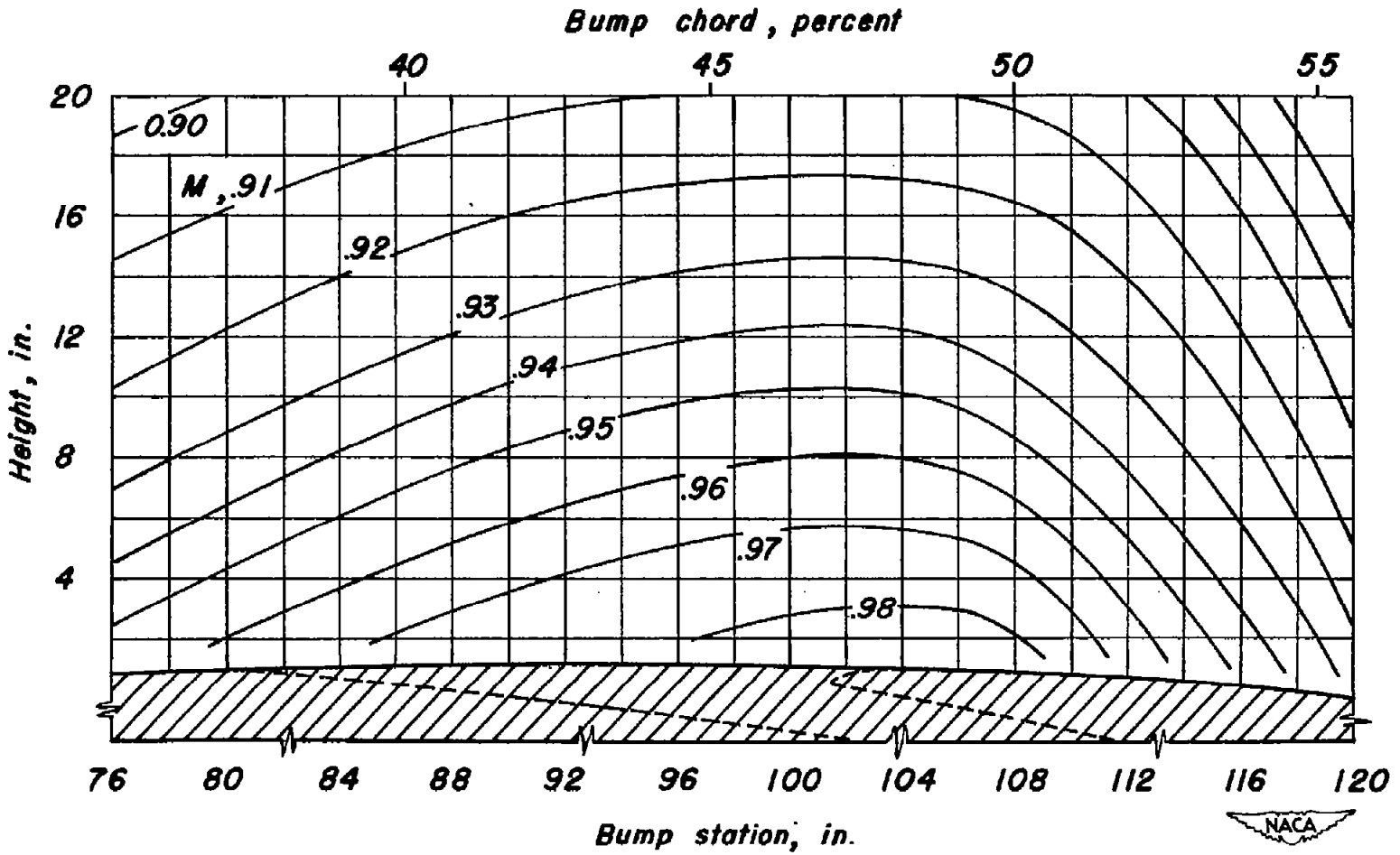

(b) M_o, 0.97.

Figure 4.- Continued.

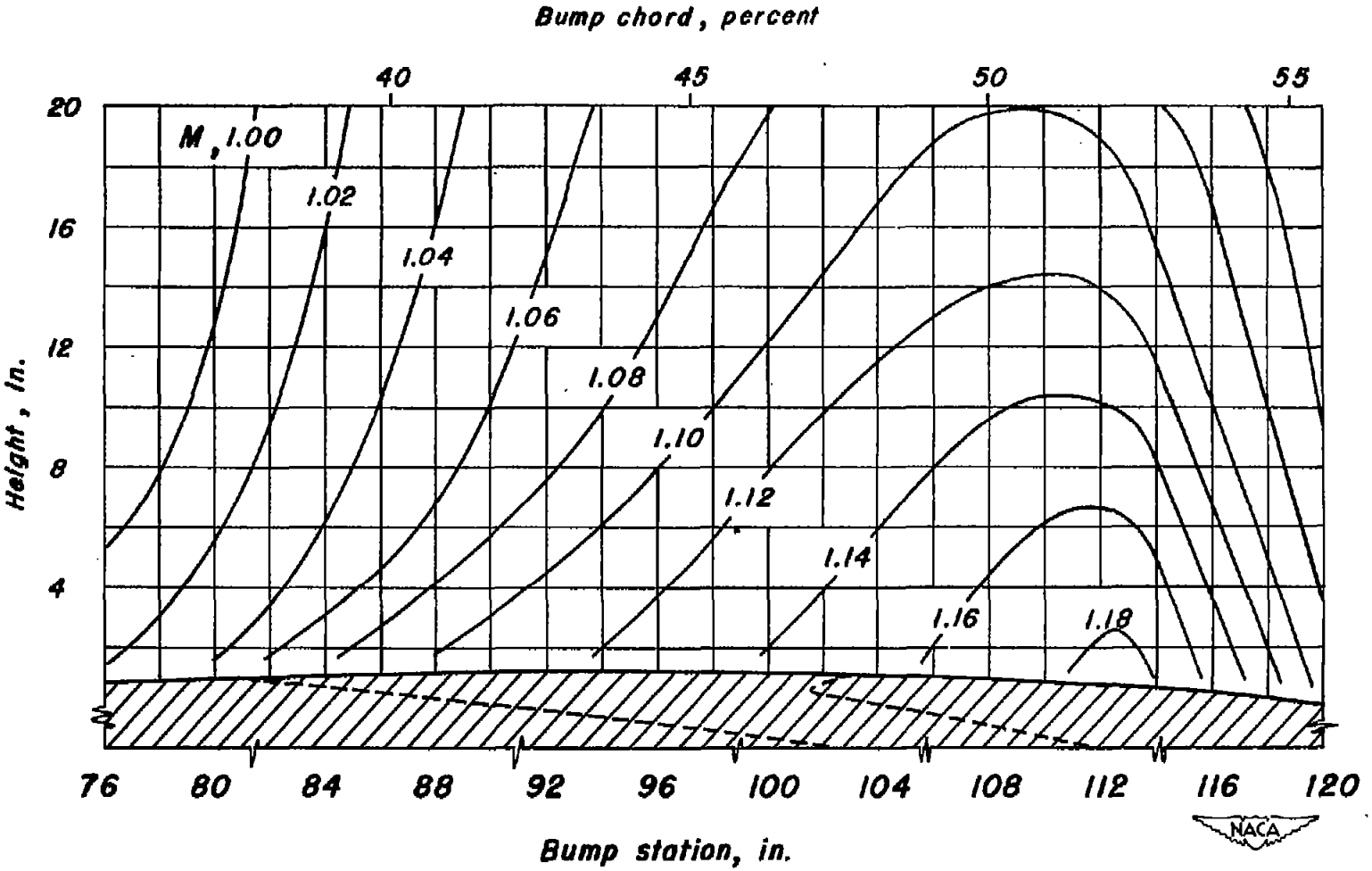

(c) M_o, 1.12.

Figure 4.- Concluded.

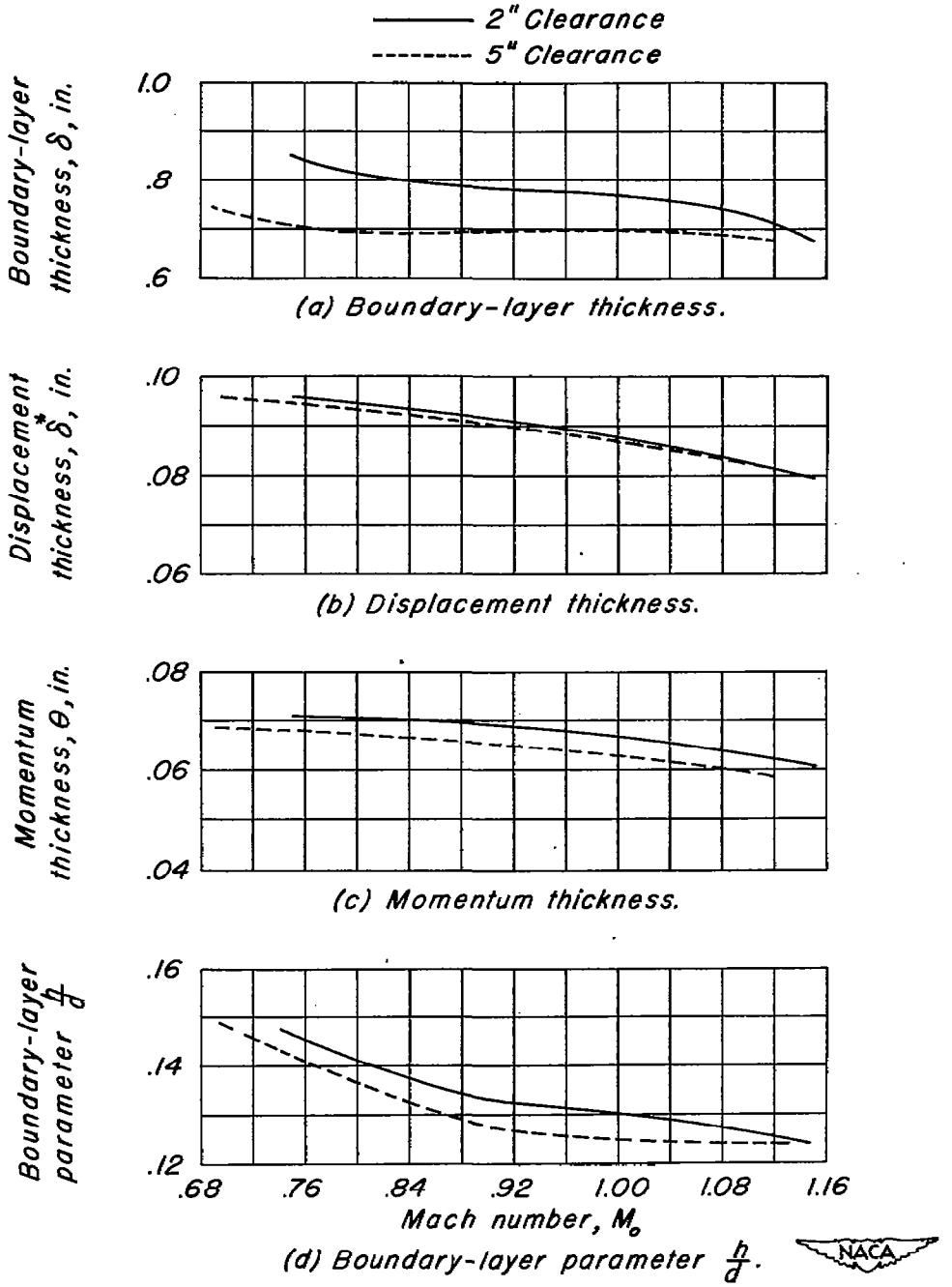

Figure 5.- Variation with Mach number of the bump boundary-layer characteristics measured at 34-percent chord for two clearances between the bump and wind-tunnel wall.

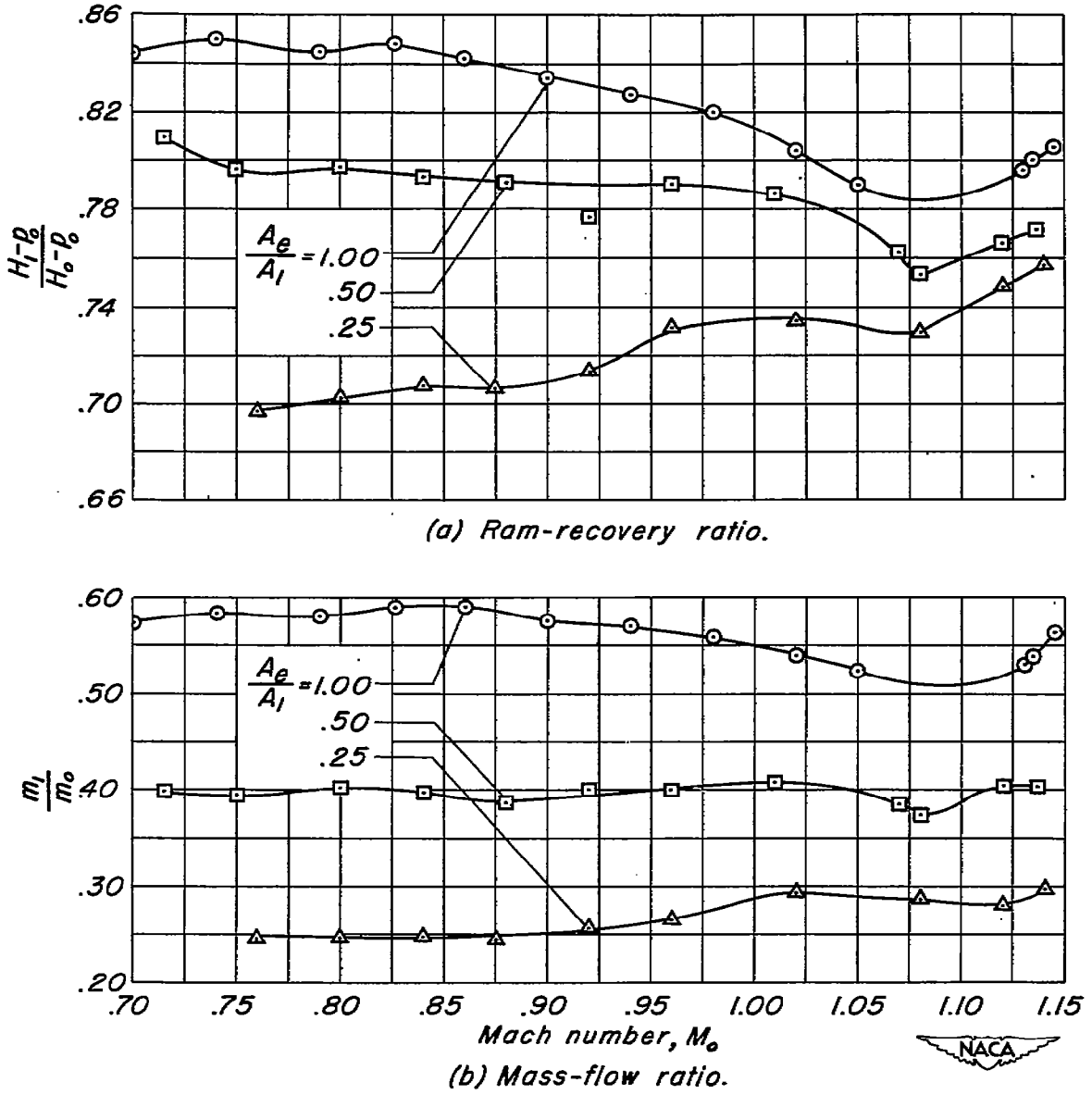

Figure 6.- Variation of ram-recovery ratio and mass-flow ratio with Mach number for three diffuser-inlet area ratios. α, 0°.

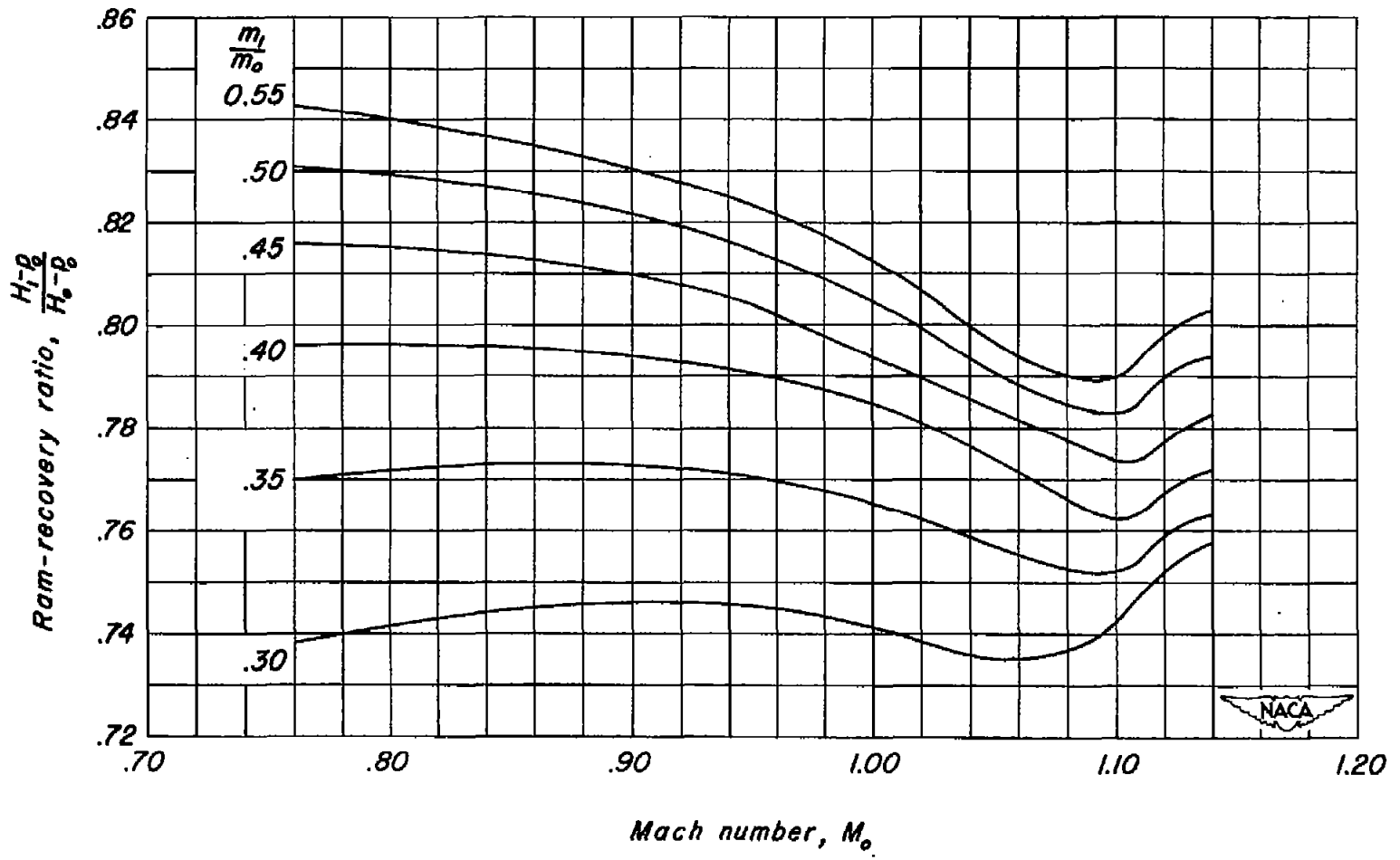

Figure 7.- Variation of ram-recovery ratio with Mach number for several mass-flow ratios. α, 0°.

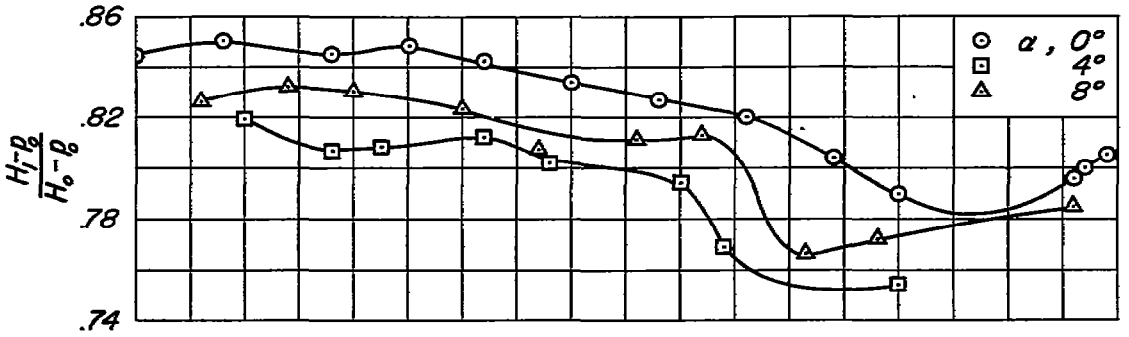

(a) Ram-recovery ratio.

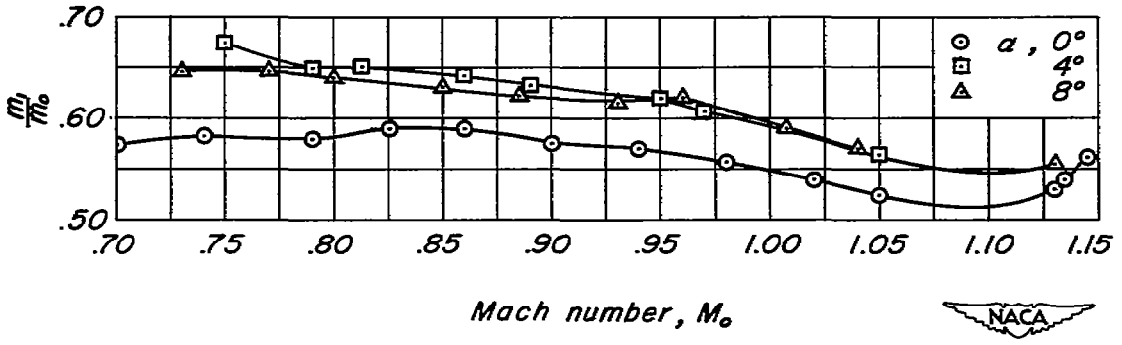

(b) Mass-flow ratio.

Figure 8.- Variation of ram-recovery ratio and mass-flow ratio with Mach number for angles of attack of 0°, 4°, and 8°.

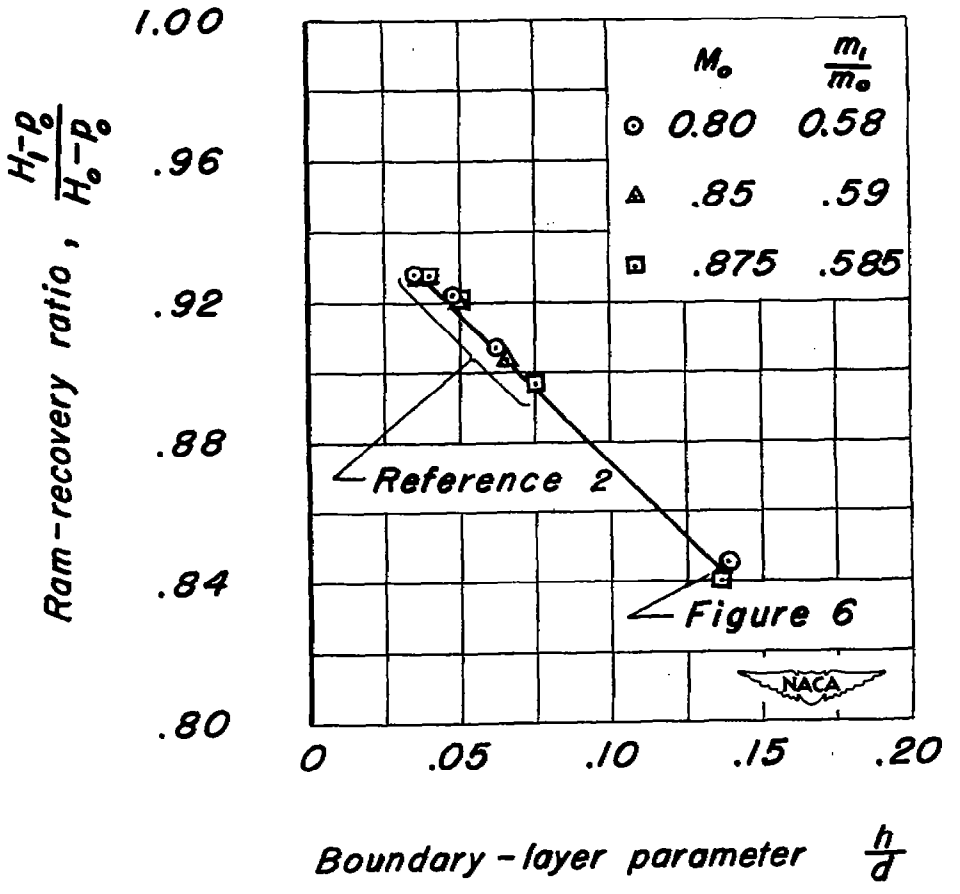

Figure 9.- Variation of ram-recovery ratio with boundary-layer parameter $\frac{h}{d}$. α, 0°.

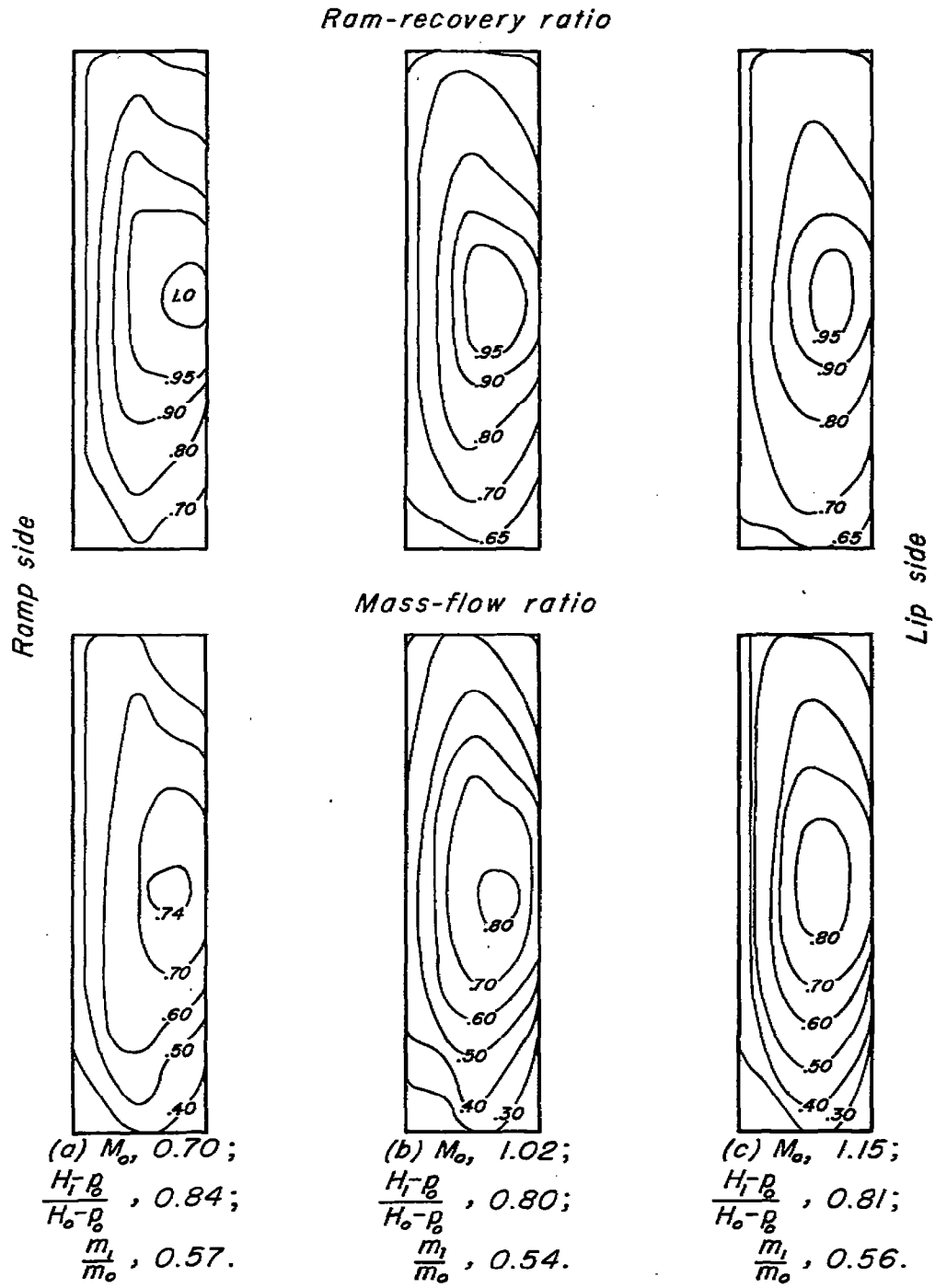

Figure 10.- Ram-recovery and mass-flow contours in the entrance of the submerged inlet, α, 0°.

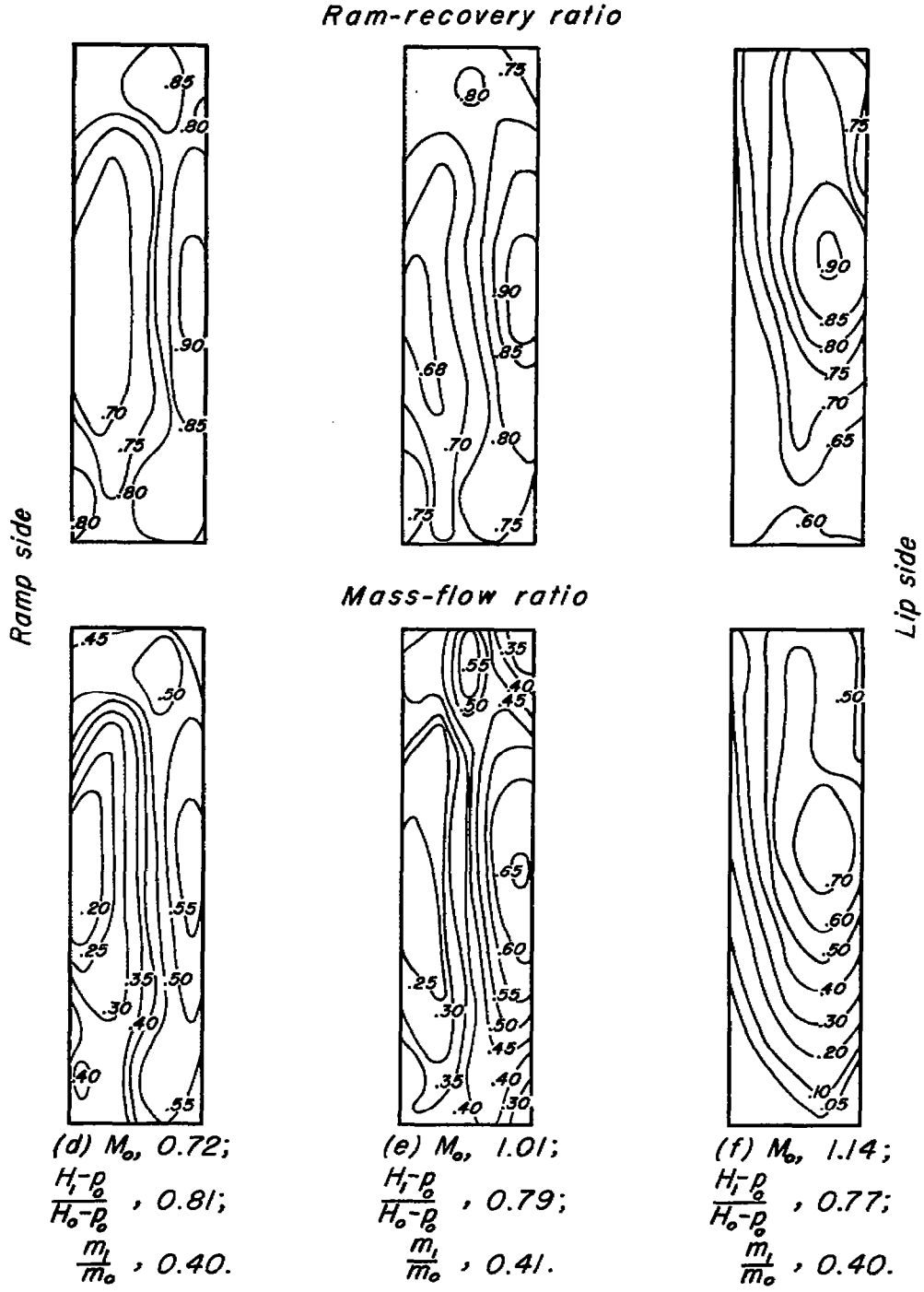

(d) M_o, 0.72; $\frac{H_1-p_o}{H_o-p_o}$, 0.81; $\frac{m_1}{m_o}$, 0.40.

(e) M_o, 1.01; $\frac{H_1-p_o}{H_o-p_o}$, 0.79; $\frac{m_1}{m_o}$, 0.41.

(f) M_o, 1.14; $\frac{H_1-p_o}{H_o-p_o}$, 0.77; $\frac{m_1}{m_o}$, 0.40.

Figure 10.- Continued.

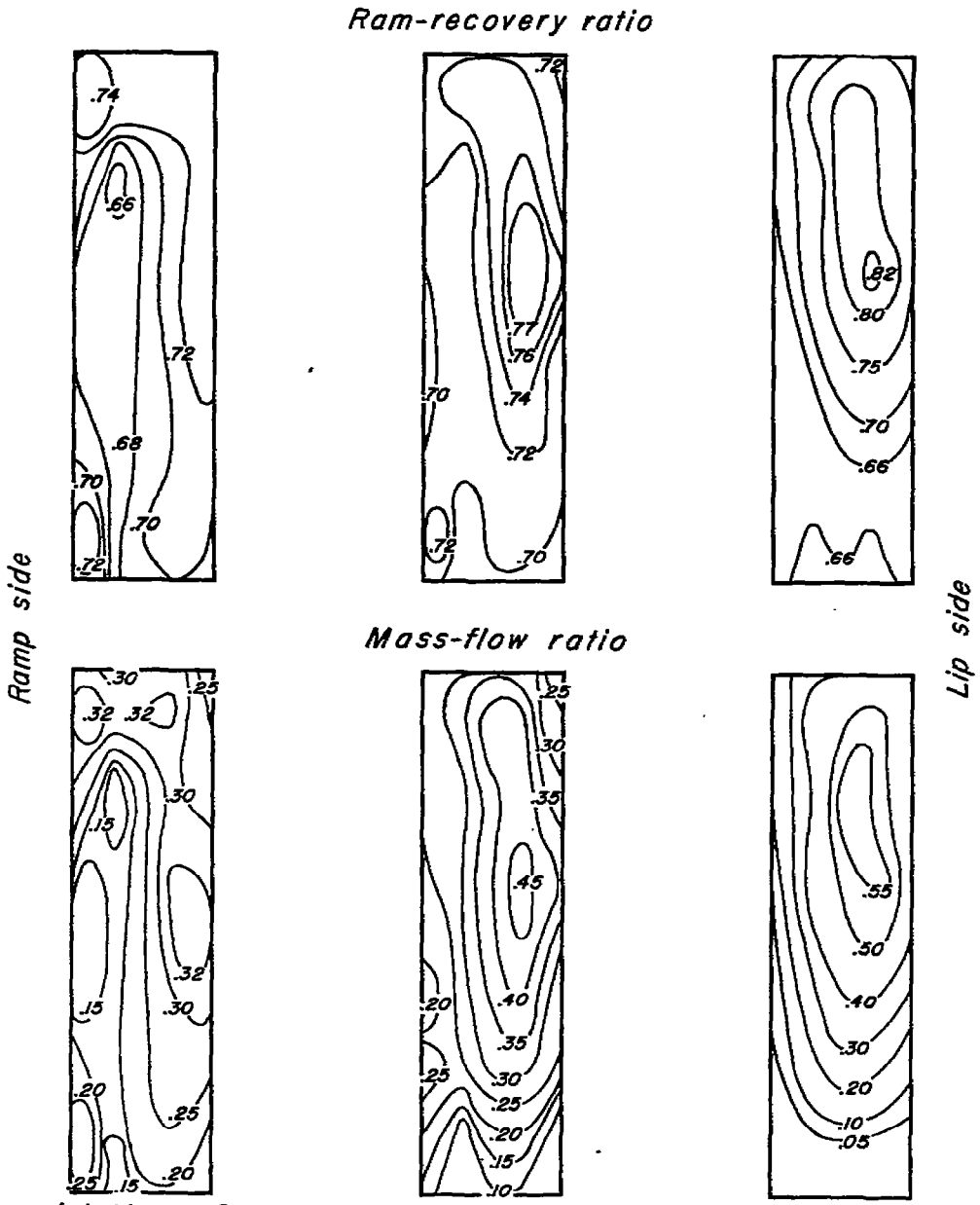

(g) M_o, 0.76; $\frac{H_1-p_o}{H_o-p_o}$, 0.70; $\frac{m_1}{m_o}$, 0.25.

(h) M_o, 1.02; $\frac{H_1-p_o}{H_o-p_o}$, 0.73; $\frac{m_1}{m_o}$, 0.29.

(i) M_o, 1.14; $\frac{H_1-p_o}{H_o-p_o}$, 0.76; $\frac{m_1}{m_o}$, 0.30.

Figure 10.- Concluded.

[redacted]

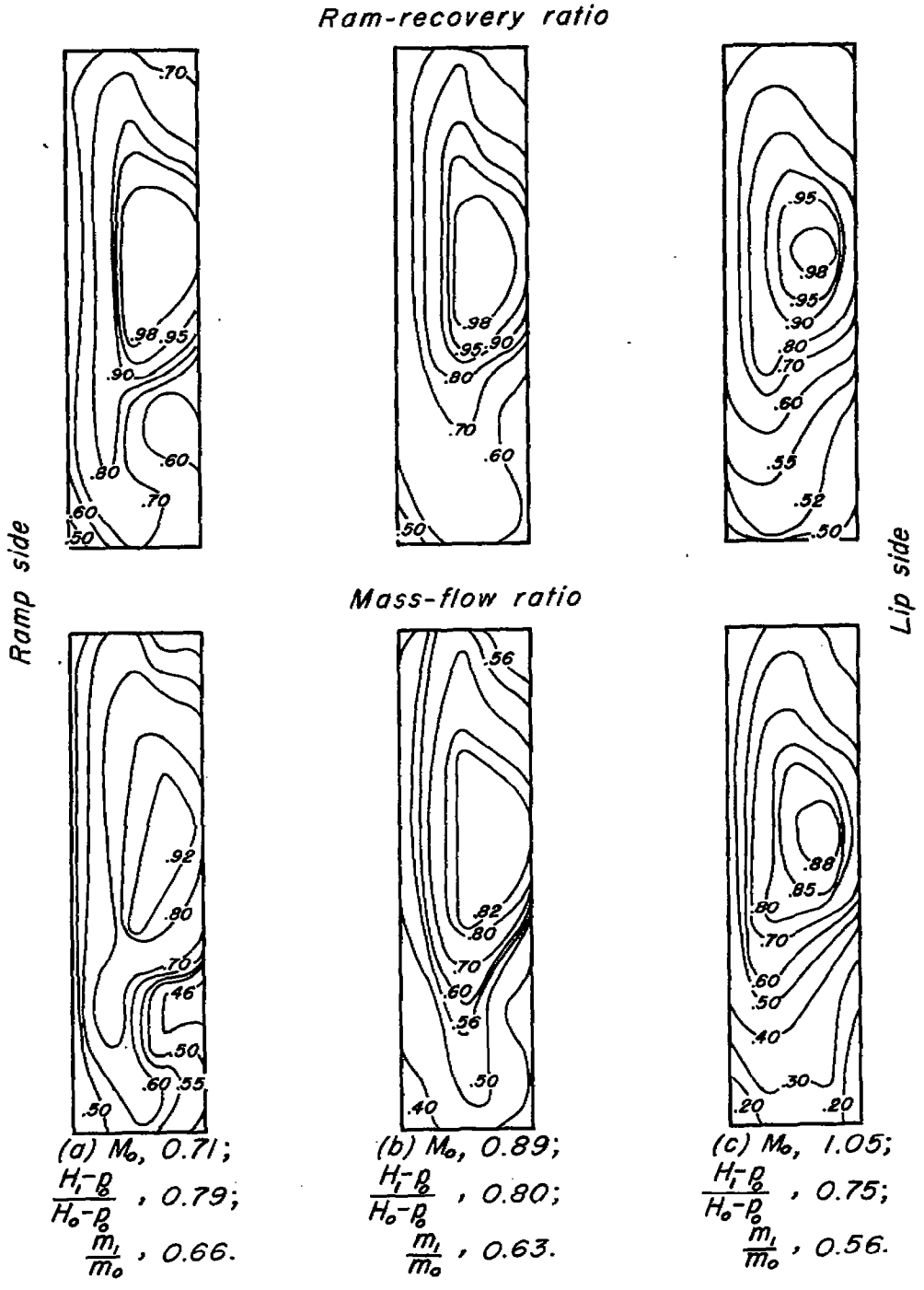

(a) M_o, 0.71; $\frac{H_1-p_o}{H_o-p_o}$, 0.79; $\frac{m_1}{m_o}$, 0.66.

(b) M_o, 0.89; $\frac{H_1-p_o}{H_o-p_o}$, 0.80; $\frac{m_1}{m_o}$, 0.63.

(c) M_o, 1.05; $\frac{H_1-p_o}{H_o-p_o}$, 0.75; $\frac{m_1}{m_o}$, 0.56.

Figure 11.- Ram-recovery and mass-flow contours in the entrance of the submerged inlet. α, 4°.

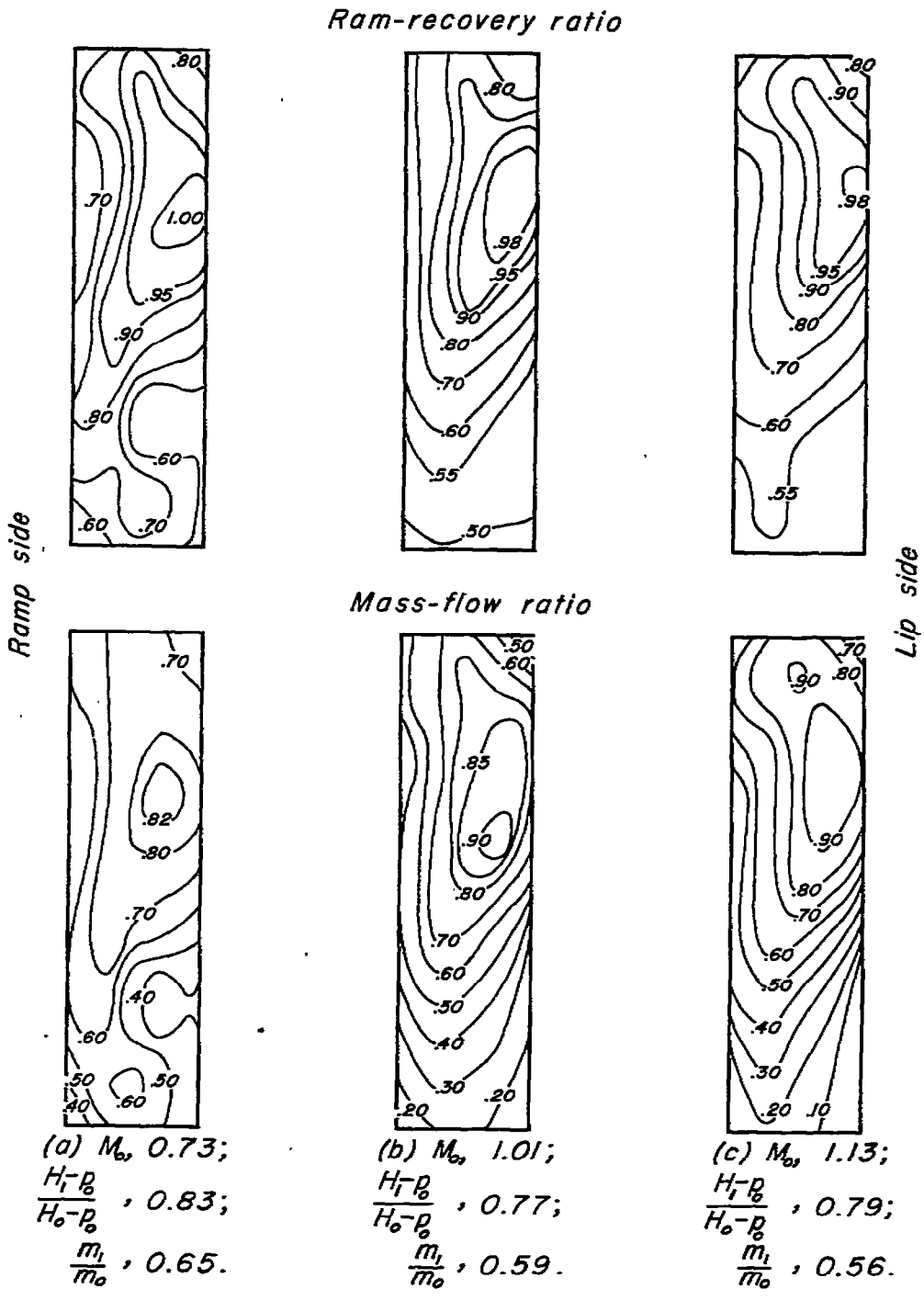

Figure 12.- Ram-recovery and mass-flow contours in the entrance of the submerged inlet. α, 8°.

[redacted]

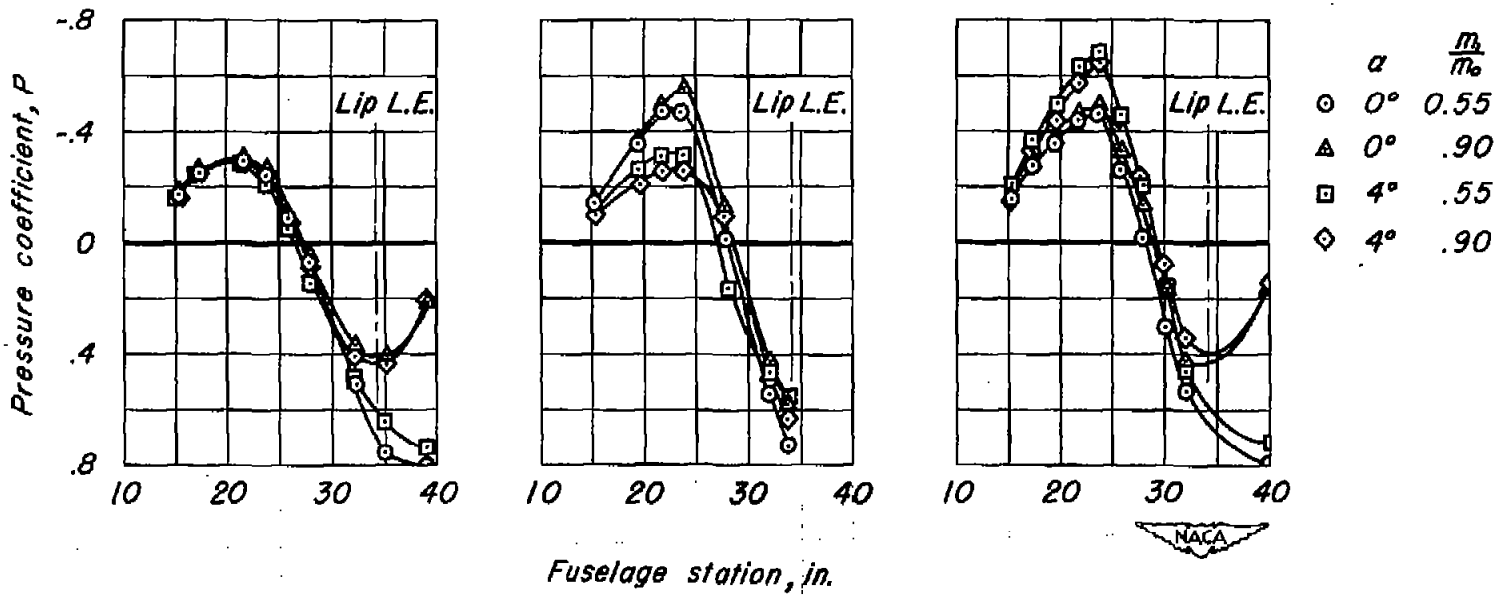

(a) Ramp. (b) Upper wall. (c) Lower wall.

Figure 13.- Pressure distribution along ramp and diverging ramp walls from investigation reported in reference 2. M_o, 0.80.

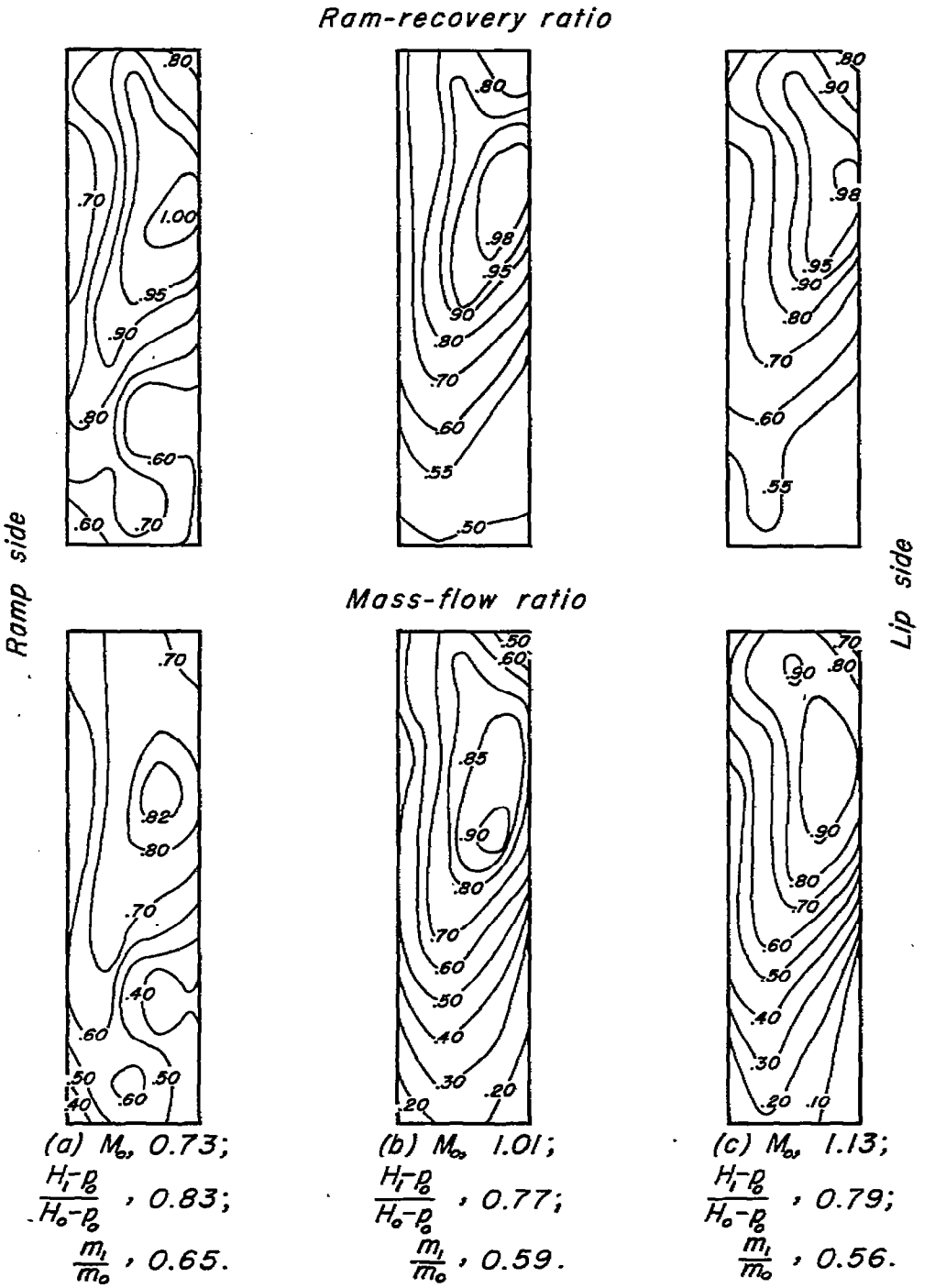

(a) M_∞, 0.73; $\frac{H_1-p_0}{H_0-p_0}$, 0.83; $\frac{m_1}{m_0}$, 0.65.

(b) M_∞ 1.01; $\frac{H_1-p_0}{H_0-p_0}$, 0.77; $\frac{m_1}{m_0}$, 0.59.

(c) M_∞, 1.13; $\frac{H_1-p_0}{H_0-p_0}$, 0.79; $\frac{m_1}{m_0}$, 0.56.

Figure 12.- Ram-recovery and mass-flow contours in the entrance of the submerged inlet. α, 8°.

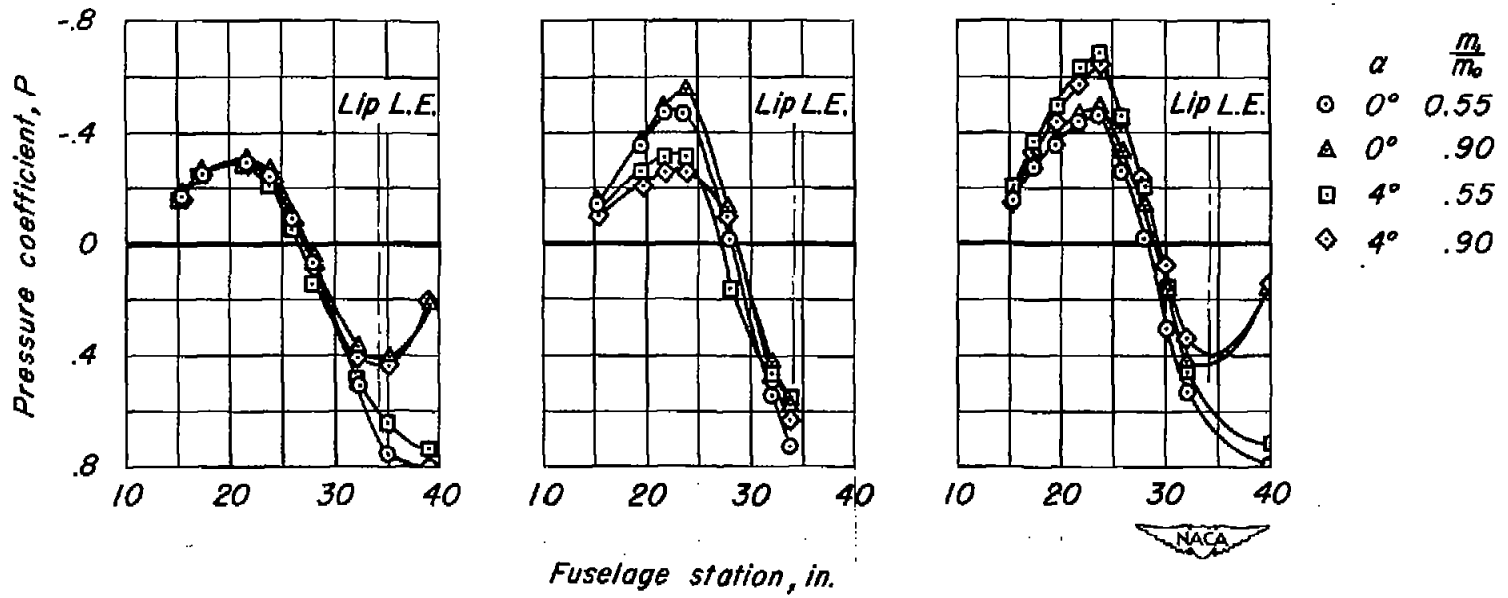

(a) Ramp. (b) Upper wall. (c) Lower wall.

Figure 13.- Pressure distribution along ramp and diverging ramp walls from investigation reported in reference 2. M_0, 0.80.

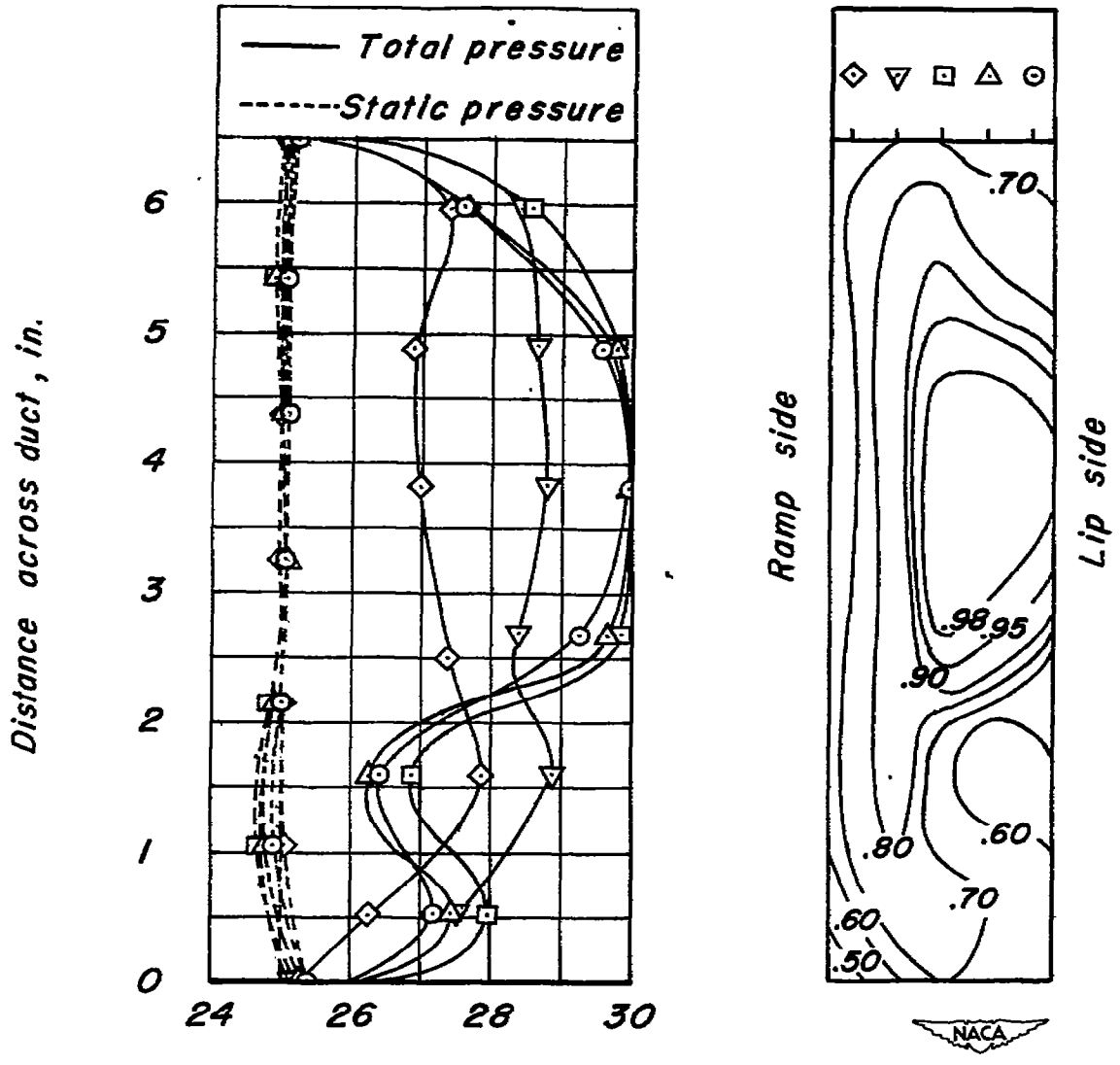

Figure 14.- Comparison of local pressures and ram-recovery ratios within the inlet. M_o, 0.71; α, 4°; $\frac{H_1-p_o}{H_o-p_o}$, 0.79; $\frac{m_1}{m_o}$, 0.66.

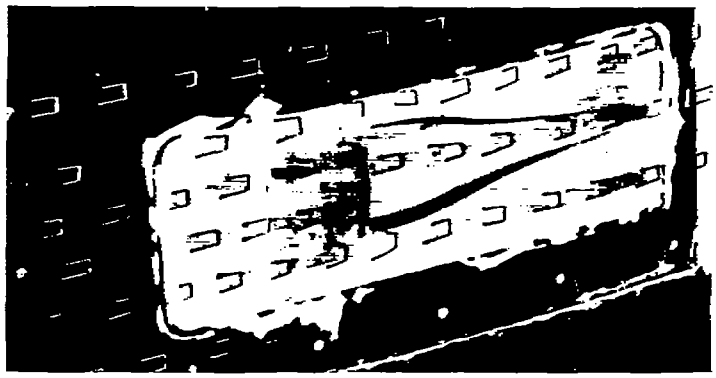

(a) M_o, 0.78; $\frac{m_1}{m_o}$, 0.58.

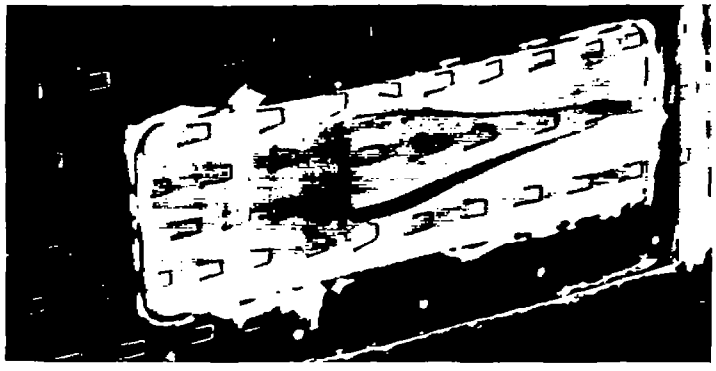

(b) M_o, 0.96; $\frac{m_1}{m_o}$, 0.56.

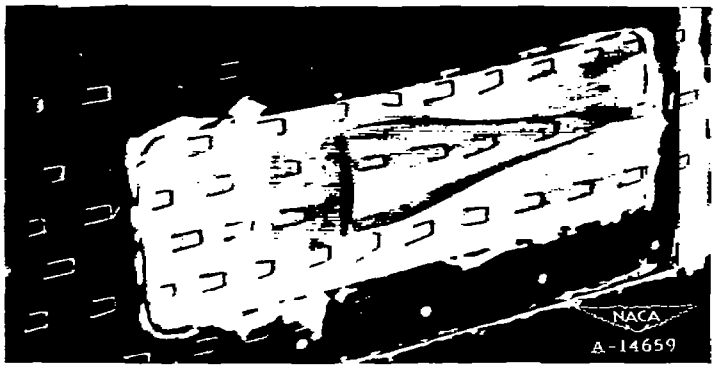

(c) M_o, 1.05; $\frac{m_1}{m_o}$, 0.53.

Figure 15.- Tufts on the submerged-inlet model at several Mach numbers. α, 0°.

(d) M_o, 1.13; $\frac{m_1}{m_o}$, 0.53.

(e) M_o, 1.15; $\frac{m_1}{m_o}$, 0.57.

Figure 15.– Concluded.

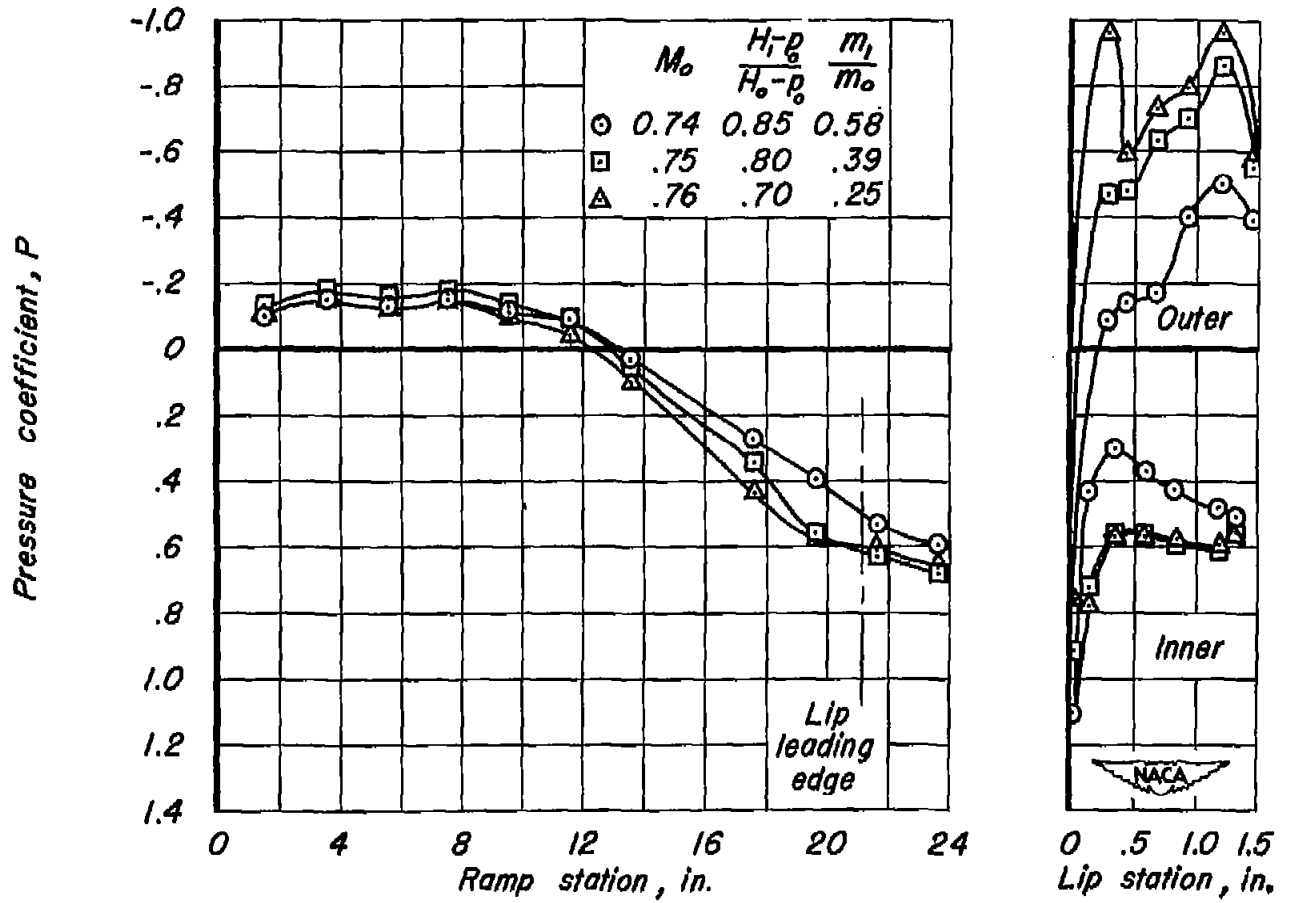

(a) Ramp pressure distribution.

(b) Lip pressure distribution.

Figure 16.- Ramp and lip pressure distributions for several mass-flow ratios and Mach numbers; α, 0°.

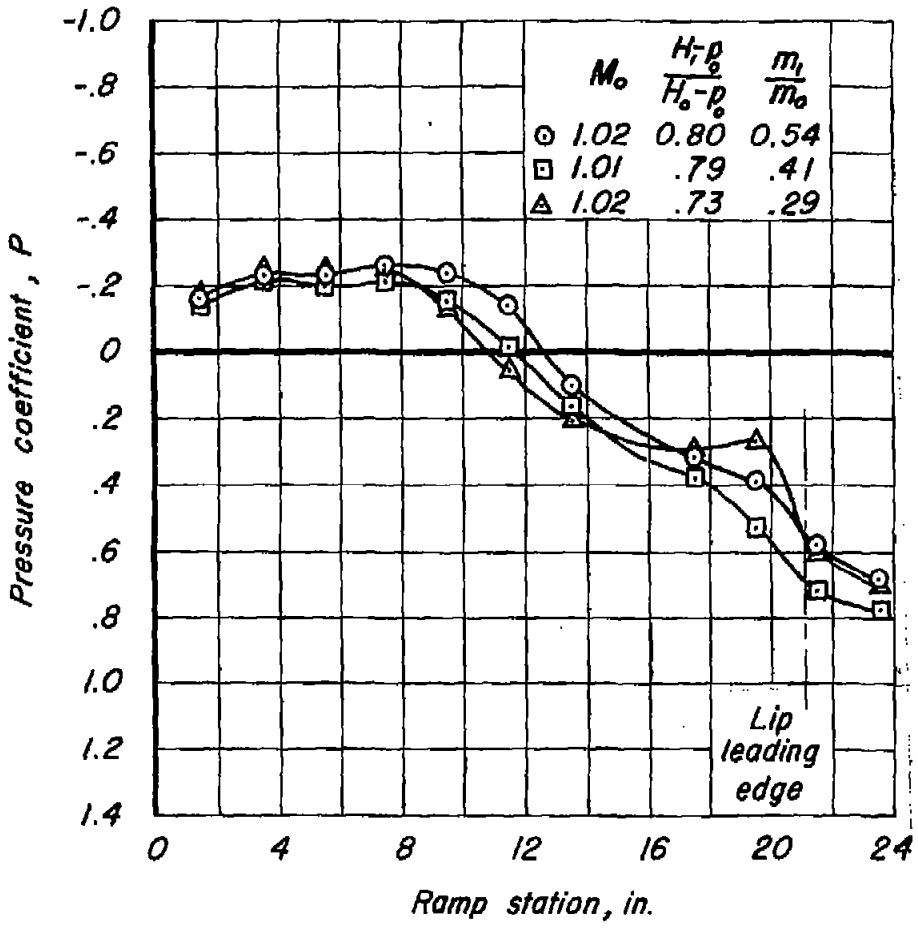

(c) Ramp pressure distribution.

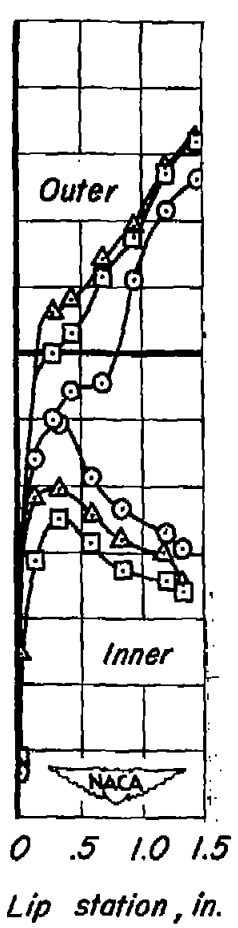

(d) Lip pressure distribution.

Figure 16.- Continued.

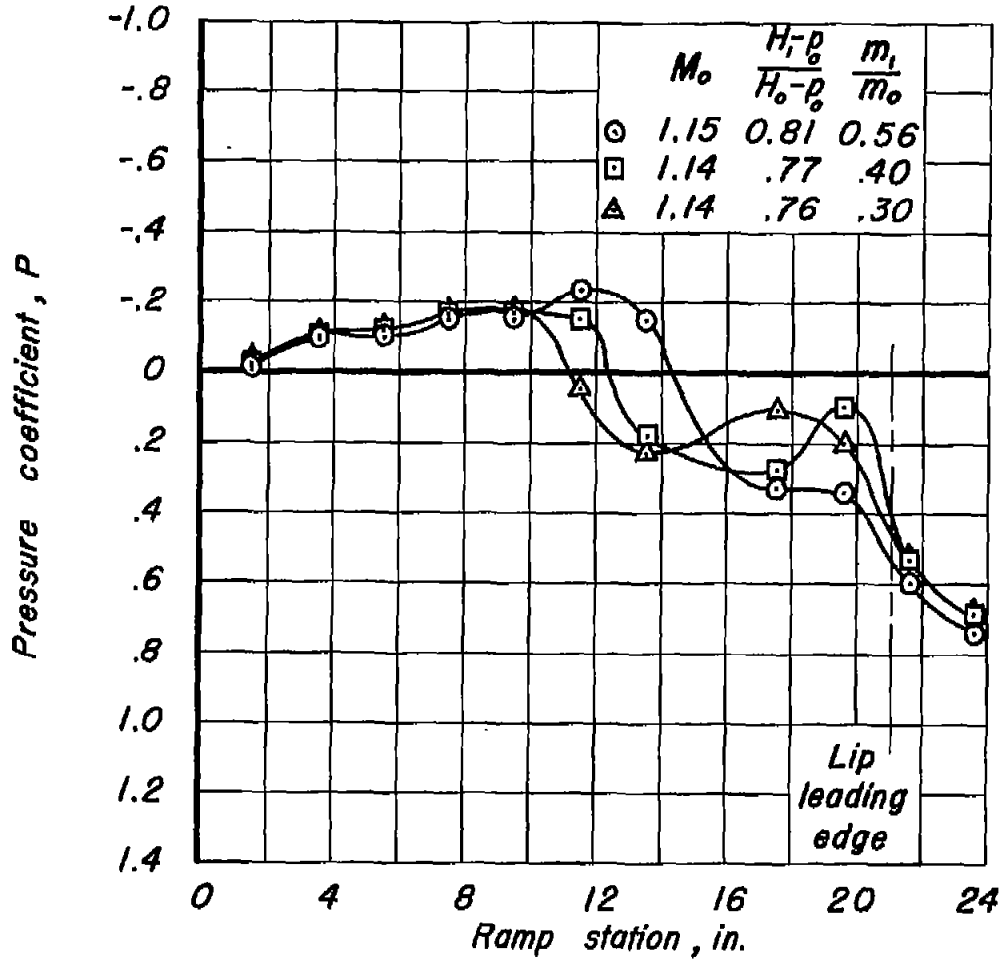

(e) Ramp pressure distribution.

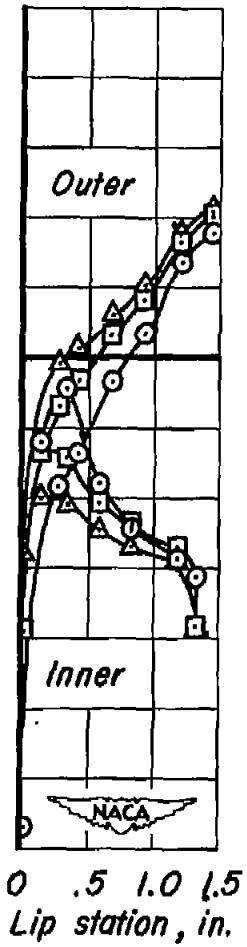

(f) Lip pressure distribution.

Figure 16.- Concluded.

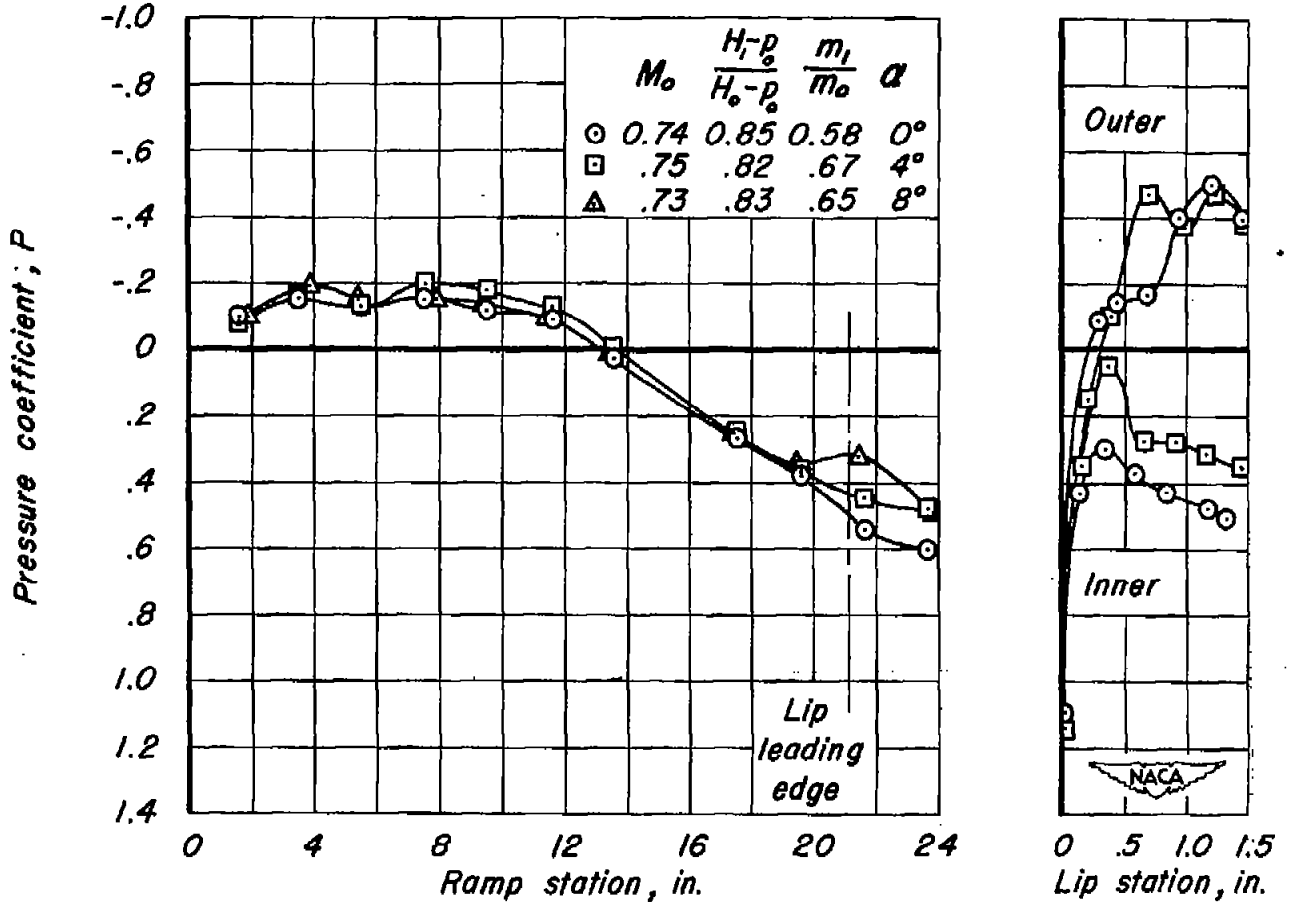

(a) Ramp pressure distribution.

(b) Lip pressure distribution.

Figure 17.- Ramp and lip pressure distributions for three angles of attack at various Mach numbers.

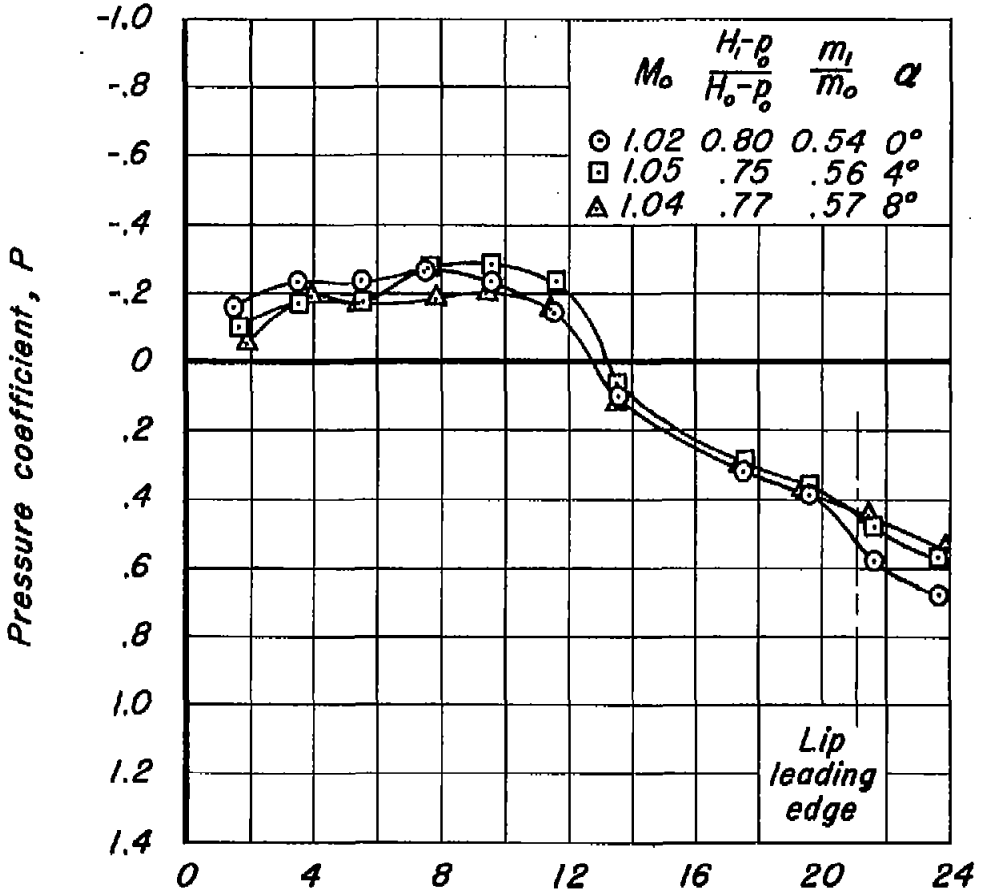

(c) Ramp pressure distribution.

(d) Lip pressure distribution.

Figure 17.- Continued.

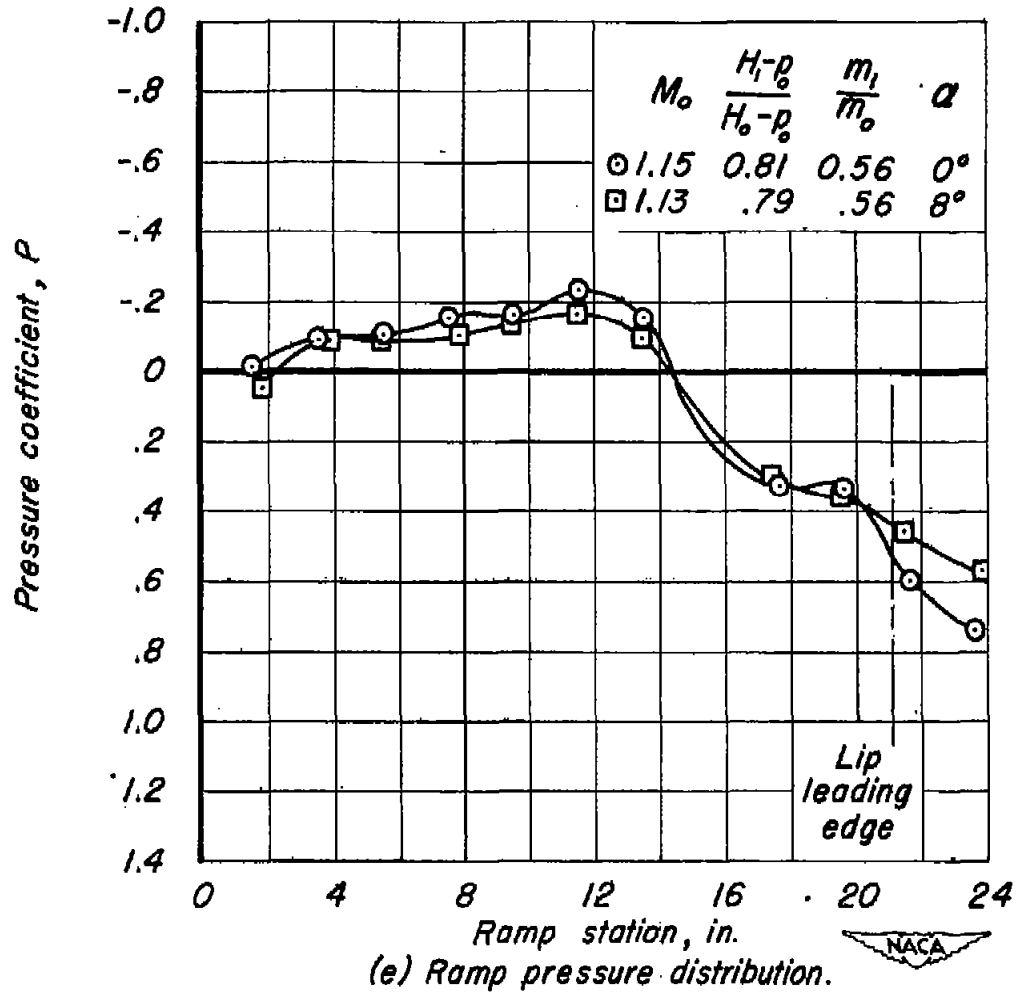

(e) Ramp pressure distribution.

Figure 17.- Concluded.